Miner Deposita (2007) 42: 465–487
DOI 10.1007/s00126-006-0071-9

ARTICLE

Alan J. Wilson · David R. Cooke · Benjamin J. Harper · Cari L. Deyell

Sulfur isotopic zonation in the Cadia district, southeastern Australia: exploration significance and implications for the genesis of alkalic porphyry gold–copper deposits

Received: 20 December 2004 / Accepted: 7 May 2006 / Published online: 11 July 2006

Abstract The alkalic porphyry gold–copper deposits of the Cadia district occur in the eastern Lachlan Fold Belt of New South Wales, Australia. The district comprises four porphyry deposits (Ridgeway, Cadia Quarry, Cadia Hill, and Cadia East) and two iron–copper–gold skarn deposits (Big Cadia and Little Cadia). Almost 1,000 tonnes of contained gold and more than four million tonnes of copper have been discovered in these systems, making Cadia the world's largest known alkalic porphyry district, in terms of contained gold. Porphyry gold–copper ore at Cadia is associated with quartz monzonite intrusive complexes, and is hosted by central stockwork and sheeted quartz–sulfide–(carbonate) vein systems. The Cadia porphyry deposits are characterized by cores of potassic and/or calc–potassic alteration assemblages, and peripheral halos of propylitic alteration, with late-stage phyllic alteration mostly restricted to fault zones. Hematite dusting is an important component of the propylitic alteration assemblage, and has produced a distinctive reddening of feldspar minerals in the volcanic wall rocks around the mineralized centers. Sulfide mineralization is strongly zoned at Ridgeway and Cadia East, with bornite-rich cores surrounded by chalcopyrite-rich halos and peripheral zones of pyrite mineralization. The Cadia Hill and Cadia Quarry deposits have chalcopyrite-rich cores and pyrite-rich halos, and Cadia Hill contains a high-level bornite-rich zone. Distinctive sulfur isotopic zonation patterns have been identified at Ridgeway, Cadia Hill, and Cadia East. The deposit cores are characterized by low $\delta^{34}S_{sulfide}$ values (−10 to −4‰), consistent with sulfide precipitation from an oxidized (sulfate-predominant) magmatic fluid at 450 to 400°C. Pyrite grains that occur in the propylitic alteration halos typically have $\delta^{34}S_{sulfide}$ values near 0‰. There is a gradual increase in $\delta^{34}S_{sulfide}$ values outwards from the deposit cores through the propylitic halos. Water–rock interaction during propylitic alteration caused magmatic sulfate reduction and concomitant oxidation of ferrous iron-bearing minerals, resulting in enrichment of ^{34}S in pyrite and also producing the distinctive reddened, hematite-rich alteration halos to the Cadia deposits. These results show that sulfur isotope analyses have potential applications in the exploration of alkalic porphyry-style deposits, with zones of depleted $\delta^{34}S_{sulfide}$ values most prospective for high-grade mineralization.

Keywords Sulfur isotopes · Gold–copper porphyry · Alkalic porphyry systems · Cadia · Lachlan orogen · Australia

Editorial handling: F. Bierlein

A. J. Wilson (✉) · D. R. Cooke · B. J. Harper · C. L. Deyell
CODES—The Australian Research Council's Centre of Excellence in Ore Deposits,
University of Tasmania,
Private Bag 79,
Hobart, Tasmania 7001, Australia
e-mail: alanwilson@angloamerican.com.au
e-mail: d.cooke@utas.edu.au
e-mail: cdeyell@utas.edu.au

A. J. Wilson
Anglo American Exploration (Australia) Pty Ltd,
Suite 1, 16 Brodie Hall Drive,
Bentley, WA 6102, Australia

B. J. Harper
Newcrest Mining Limited,
Cadia Road,
Orange, NSW 2800, Australia

Introduction

Porphyry gold–copper deposits of the Cadia and Goonumbla districts are currently eastern Australia's most significant gold producers and also produce important quantities of copper. These deposits formed within an Ordovician oceanic island arc setting known as the "Macquarie Arc" (Glen and Walshe 1999; Fig. 1), part of the Paleozoic Lachlan Fold Belt. The porphyry gold–copper deposits at Cadia and Goonumbla are classified as "alkalic" porphyry systems and formed within two late Ordovician submarine volcanic centers of shoshonitic character (Fig. 2; Cooke et al. 2007). Although the Goonumbla deposits were the first to be

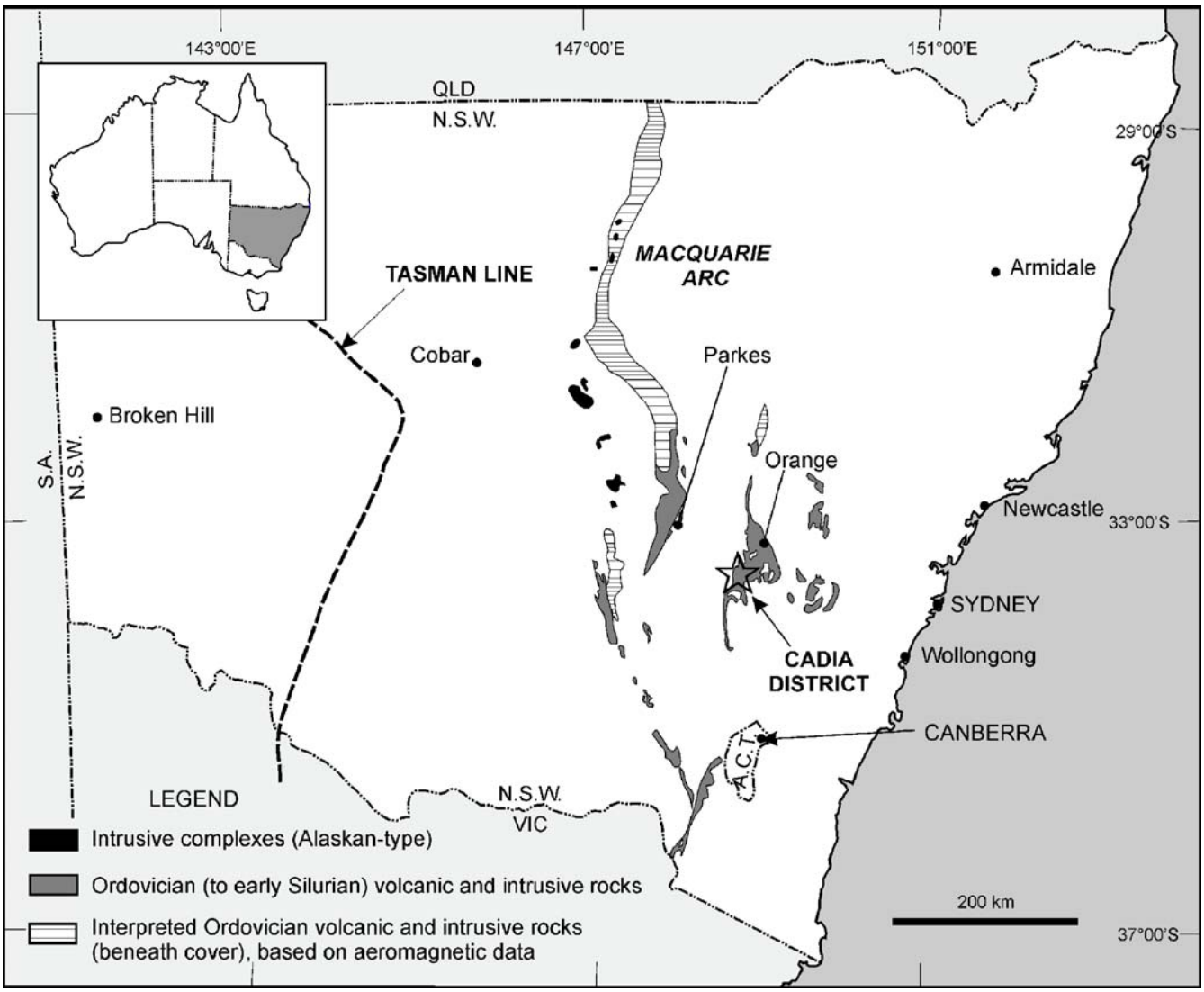

Fig. 1 Locality map, Lachlan Fold Belt, Eastern Australia (modified after Holliday et al. 2002)

discovered, the Cadia systems are larger in terms of contained gold. The Cadia district hosts four alkalic porphyry gold–copper deposits (Ridgeway, Cadia Quarry, Cadia Hill, and Cadia East; Fig. 3; Table 1), and contains a combined total of more than 980 tonnes of gold. The Ridgeway deposit has an exceptional average gold grade for a porphyry system (1.9 g/t; Table 1), making it an extremely attractive exploration target.

Alteration footprints have generally proven to be the most useful guide in porphyry exploration due to the enormous volumes of rock that are typically affected by magmatic–hydrothermal fluids, and the distinctive mineral assemblages that can be produced via water–rock interaction (e.g., Lowell and Guilbert 1970; Titley 1982). K-feldspar, biotite, and magnetite altered rocks (the "potassic" or "K-silicate" alteration assemblage) host ore in many porphyry systems. These alteration assemblages occur within the intrusions and surrounding wallrocks. Porphyry deposits also have peripheral halos of chlorite, epidote, calcite, and albite-altered rocks ("propylitic" assemblage), which can extend for kilometers laterally from the central intrusive complex. In calc–alkalic porphyry systems, late-stage alteration by acidic fluids can produce extensive domains of phyllic, argillic, intermediate, and advanced argillic alteration. However, in alkalic systems, these alteration assemblages are typically lacking, or are restricted to narrow zones around late-stage faults (Drummond and Godwin 1976; Lickfold et al. 2003; Cooke et al. 2007). Consequently, explorers for potentially high-grade alkalic porphyry deposits have to contend with subtle and complicated overprinting relationships between propylitic and potassic alteration assemblages (e.g., Lang et al. 1995) that limit the effectiveness of alteration zonation as an exploration tool.

The sulfur isotopic compositions of sulfide minerals in porphyry deposits are typically reported to be near-zero, and of magmatic derivation (e.g., Ohmoto 1986; Taylor 1987). Lower values of $\delta^{34}S_{sulfide}$ can occur when there is an abundance of oxidized sulfur in the hydrothermal fluid, due to isotopic fractionation between oxidized and reduced aqueous sulfur species (Rye et al. 1992; Rye 1993). Several

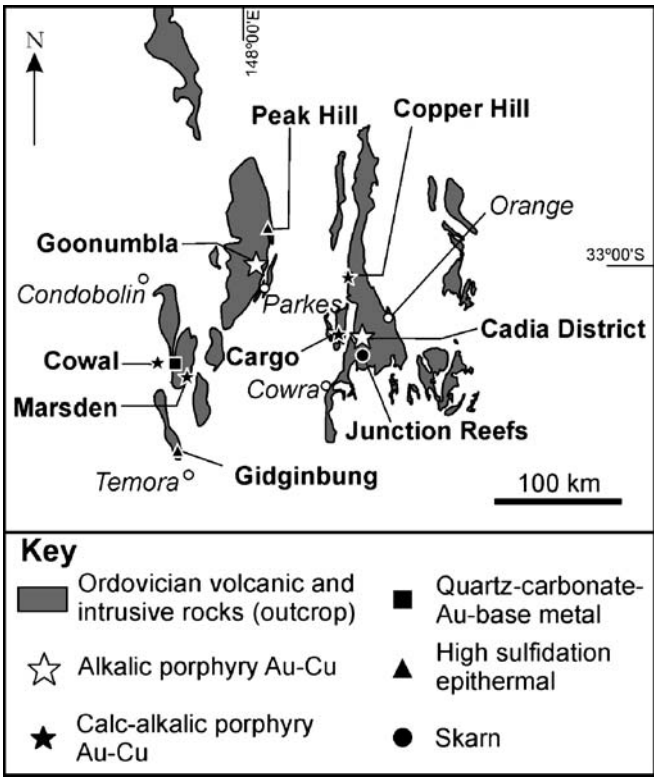

Fig. 2 Present-day distribution of volcanic and volcaniclastic rocks of the Ordovician Macquarie Arc in NSW, showing the location of selected Ordovician mineral districts and deposits (modified after Holliday et al. 2002)

alkalic porphyry deposits are characterized by sulfide mineralization with distinctively negative sulfur isotopic compositions. At Galore Creek (British Columbia), $\delta^{34}S_{sulfide}$ values range between −7 and −13‰ (Shannon et al. 1983). Similar results have been obtained from Goonumbla (+0.7 to −19.7‰; Lickfold 2002), where isotopic compositions range from strongly negative values in the bornite-rich cores of the deposits to higher values in the pyrite-bearing propylitic halo (Heithersay and Walshe 1995; Radclyffe 1995; Lickfold 2002).

This paper investigates the potential use of sulfur isotopic zonation as an exploration tool for high-grade mineralization in alkalic porphyry systems, based on our analytical results from three alkalic porphyry gold–copper deposits in the Cadia district. Mechanisms for the sulfur isotopic evolution of hydrothermal fluids and sulfide mineralization in the Cadia systems are also evaluated, and their implications for porphyry ore genesis are discussed.

Geology of the Cadia district

The geology of the Cadia district has been described by Holliday et al. (2002) and Wilson et al. (2003), and is shown in Fig. 3. The oldest rocks in the district are part of the Weemalla Formation, a mid-late Ordovician sequence of fine grained, laminated, volcaniclastic siltstones deposited in a sub-wave base environment (Packham et al. 1999). The Weemalla Formation crops out on the western side of the Cadia district (Fig. 3) and hosts gold–copper mineralization in the deeper parts of the Ridgeway deposit (Fig. 4a).

The Forest Reefs Volcanics conformably overlie the Weemalla Formation (Figs. 3 and 4a), and comprise a package of volcaniclastic conglomerates, sandstones, shoshonitic volcanic rocks, and minor limestones. The volcanic rocks and volcanic detritus are dominated by primary feldspars, clinopyroxene, and magnetite. Rare conodont fauna indicate deposition during the Eastonian (Packham et al. 1999), which is approximately 450–448 Ma according to the time scale of Cooper (1999). The Forest Reefs Volcanics are the major host rock at Cadia East and Ridgeway, and host minor volumes of ore at Cadia Hill and Cadia Quarry (Fig. 4).

Swarms of pyroxene- and plagioclase-phyric dykes have intruded the Forest Reefs Volcanics. Individual dykes are up to 25 m thick. The dykes intruded during the late Ordovician because they are overprinted by late Ordovician to early Silurian porphyry-style mineralization and alteration at Cadia East and Ridgeway (Fig. 4a,d).

Monzodioritic to monzonitic intrusive complexes intruded the Weemalla Formation, the Forest Reefs Volcanics, and the pyroxene-phyric dyke swarm (Figs. 3 and 4). The intrusions are known collectively as the Cadia Intrusive Complex, and have shoshonitic affinities (Holliday et al. 2002). They are intimately associated with gold–copper mineralization at each of the Cadia porphyry deposits (Fig. 4). U–Pb age determinations indicate a late Ordovician–early Silurian timing (439±6 Ma; Black, 1994, unpublished report to Newcrest Mining Limited).

The Cadia district is overlain by a sequence of fine grained marine shales and siltstones of middle to late Silurian age (Wenlock to Přídolí, Rickards et al. 2001; Fig. 3). Clasts of Ordovician monzonite and skarn occur in the basal Silurian conglomerate (Green 1999), indicating that the monzonite porphyries and skarn mineralization were uplifted and exhumed by the mid-Silurian. The Silurian shale and the Forest Reefs Volcanics are overlain unconformably by Tertiary alkalic volcanic rocks of the Canobolas Volcanic Complex (Fig. 3).

The Cadia porphyry deposits lie on a six-kilometer long, WNW-trend (Fig. 4), which appears to be part of a crustal-scale lineament known as the Lachlan Transverse Zone (Glen and Walshe 1999). The Cadia Hill and Cadia Quarry deposits have been localized by the intersection of N-trending faults with the WNW-trending structure. Tertiary volcanism also appears to have been controlled by this fault architecture, implying a protracted history of fault reactivation.

Porphyry deposits

The porphyry deposits of the Cadia district have been described in detail by Harper (2000), Tedder et al. (2001), Holliday et al. (2002), Wilson (2003), Wilson et al. (2003, 2004), and their characteristics are summarized

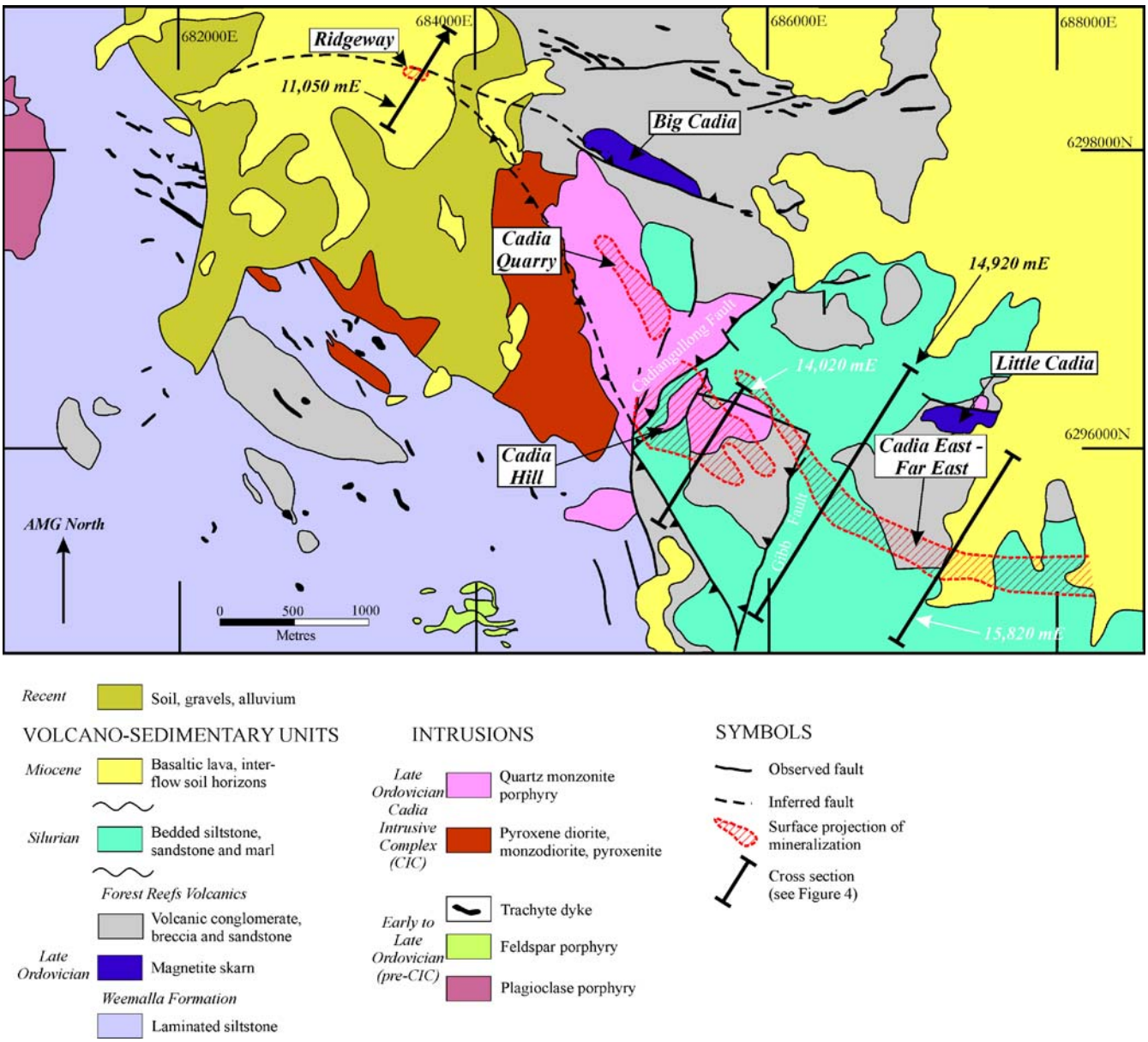

Fig. 3 Geology of the Cadia district, based on unpublished mapping by Newcrest Mining Limited and modified after Holliday et al. (2002). The locations of the four known porphyry mineral centers (Ridgeway, Cadia Quarry, Cadia Hill, and Cadia East) and iron–copper–gold skarns at Big Cadia and Little Cadia are *highlighted*, as are the cross section locations for Fig. 4

below. The location of each deposit is shown in Fig. 3; and Fig. 4 illustrates a geological cross-section through each deposit.

Ridgeway

The Ridgeway deposit was discovered in 1996 (Holliday et al. 1999), and is the highest-grade system at Cadia, containing a total resource of 77 Mt at 1.87 g/t gold and 0.63‰ copper (Table 1). Ridgeway is an underground sublevel-cave mining operation that has been in production since 2001. Wilson et al. (2003) have described the geology and mineral paragenesis of Ridgeway in detail. High-grade gold–copper mineralization is centered on a thin, pipe-like monzonite intrusive complex that was emplaced into the Weemalla Formation and Forest Reefs Volcanics (Fig. 4a). Mineralization is hosted in a series of sheeted and stockwork quartz–bornite–chalcopyrite–magnetite–calcite veins, intimately associated with potassic (orthoclase–biotite–quartz) and calc–potassic (actinolite–biotite–orthoclase) alteration assemblages (Figs. 5a and 7). The nomenclature of Wilson et al. (2003) (Early, Transitional, Late, and Peripheral) has been used in this study to identify the paragenetic stages of sulfides analyzed as part of this study. There is a halo of propylitic alteration that extends outwards from the potassic-altered core at Ridgeway (Fig. 7). The propylitic zone can be subdivided into an inner, "reddened" zone characterized by hematite-dusting of feldspars (Fig. 5b), and an outer, weakly altered zone

Table 1 Resources of the Cadia district at the end of June 2004 (Newcrest Mining Limited 2004)

Deposit		Mt	Au (g/t)	Au (t)	Cu (%)	Cu (Mt)
Cadia Hill	Total resource	265	0.67	179	0.16	0.42
Cadia Quarry	Total resource	40	0.40	16	0.21	0.09
Ridgeway	Total resource	77	1.87	144	0.63	0.49
Cadia East open pit	Total resource	300	0.46	138	0.37	1.11
Cadia East underground	Total resource	530	0.81	429	0.33	1.75
Big Cadia	Total resource	30	0.40	12	0.50	0.15
Little Cadia	Total resource	8	0.30	2	0.40	0.03
Total resource		1,212	0.75	908	0.32	3.87
Cadia Hill	Historic production			52		0.16
Ridgeway	Historic production			31		0.12
Total metal endowment of district				991		4.15

Data for Big Cadia and Little Cadia are from Holliday et al. (2002). The Cadia East underground resource includes the deposit formerly known as Cadia Far East. Also included are the total gold and copper production figures since start of mining of Cadia Hill and Ridgeway to end of June 2004

where chlorite, albite, pyrite, calcite, and prehnite are the only alteration minerals of significance (Fig. 5c).

Cadia Hill and Cadia Quarry

The Cadia Hill and Cadia Quarry deposits were discovered in 1992, and have been exploited by open pit mining since 1998. The Cadia Hill deposit has been described by Newcrest Mining Staff 1996, Holliday et al. (2002), and Wilson (2003). Wilson et al. (2004) described the geology and mineralization of Cadia Quarry. Mineralization is restricted mostly to within a large quartz monzonite body, and only locally occurs within the adjacent Forest Reefs Volcanics (Figs. 3 and 4b). The monzonitic intrusions range from medium grained, equigranular monzodiorite to coarsely orthoclase porphyritic quartz monzonite and, locally, fine grained syenite. Sheeted quartz–sulfide–calcite veins host the bulk of the mineralization. At Cadia Quarry, a small domain of high-grade copper mineralization is associated with an unusual pegmatitic breccia, in which weakly mineralized and veined monzonite fragments have been cemented by coarse-grained orthoclase, quartz, biotite, calcite, and sulfides. Early-formed sodic (albite) and potassic (biotite-orthoclase; labeled potassic I on Fig. 8) alteration assemblages have an irregular distribution throughout the deposits. Orthoclase alteration envelopes (potassic II; Fig. 8) accompany Main Stage sheeted quartz–calcite–sulfide veins (Fig. 5d). These alteration assemblages have been overprinted by propylitic (chlorite–calcite) and late-stage phyllic (illite–muscovite–pyrite) alteration. Hematite alteration envelopes occur locally around epidote veinlets within zones of propylitic alteration (Fig. 5e). Reddening of feldspars due to hematite dusting is a common feature of the potassic and propylitic alteration assemblages. Phyllic alteration is grade-destructive and is restricted to the walls of large faults, and to a late-stage quartz-fragment breccia body that has disrupted the pegmatite-cemented breccia at Cadia Quarry.

Cadia East

Cadia East (formerly known as both the Cadia East and Far East deposits) contains an inferred resource of 830 Mt at 0.69 g/t gold and 0.35‰ copper (Table 1). The deposit has been described previously by Tedder et al. (2001), Holliday et al. (2002), and Wilson (2003). Cadia East contains diverse styles of mineralization compared to the other porphyry deposits of the Cadia district. At shallow levels (100–500 m below surface), broadly stratabound copper–gold mineralization is hosted by volcaniclastic conglomerates and sandstones of the Forest Reefs Volcanics (Fig. 4c). Subjacent to this higher grade gold–copper mineralization occurs within and around a series of quartz monzonite porphyry dykes that occur at greater depths (700 to >1,500 m) in the eastern half of the deposit (Fig. 4d).

There is a complex paragenesis of alteration at Cadia East. Early stage biotite–orthoclase–magnetite alteration (potassic I; Figs. 9 and 10) has been cut by sheeted, main stage quartz–calcite–sulfide veins associated with orthoclase alteration envelopes (potassic II; Fig. 5f). At shallower depths, stratabound mineralization comprises disseminated chalcopyrite–pyrite associated with pervasive biotite ± tourmaline alteration (potassic III; Fig. 5g). A subzone of pink hematite-bearing propylitic alteration (inner propylitic; Fig. 5h) occurs between the potassic alteration zones and the peripheral subzone of propylitic alteration. In the upper levels of the deposit, all stages of potassic alteration are overprinted by zones of late stage pervasive feldspar alteration characterized by white potassium feldspar, albite, and locally abundant pyrite. Fracture and fault controlled phyllic alteration has overprinted all of the earlier formed alteration assemblages locally.

Sulfur isotopes

A systematic study of sulfur isotopic compositions of sulfides has been completed for samples from the Ridgeway, Cadia Hill, and Cadia East deposits. The samples were selected

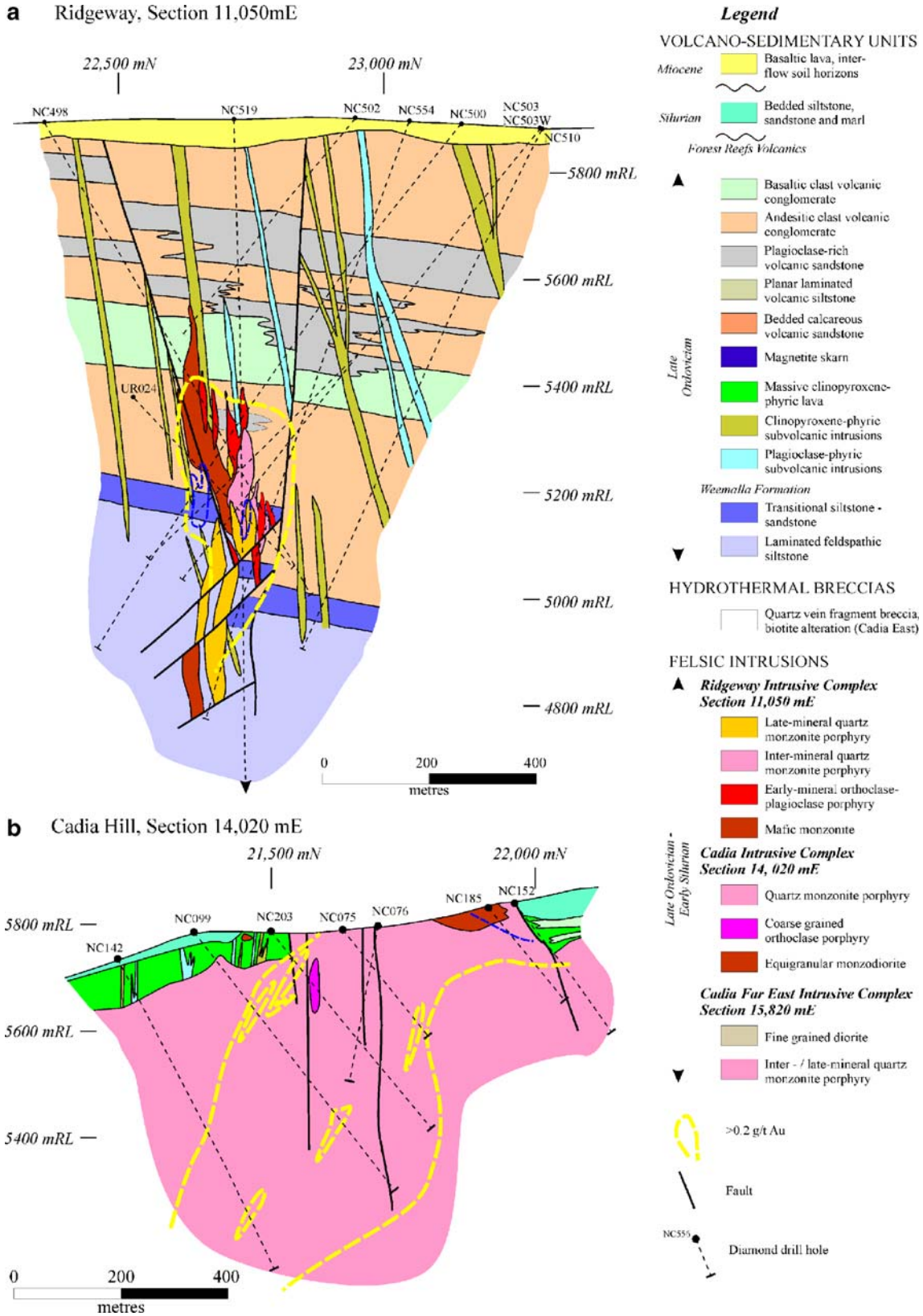

Fig. 4 Interpreted geological cross-sections through the porphyry deposits of the Cadia district. Sections based on graphical logging of drill holes as indicated and supplemented by geological information from additional drill holes on each section that were logged by Newcrest Mining Ltd. staff. **a** Ridgeway (section 11,050E); **b** Cadia Hill (section 14,020E); **c** Cadia East (section 14,920E); and **d** Cadia East (section 15,820E)

Fig. 4 (continued)

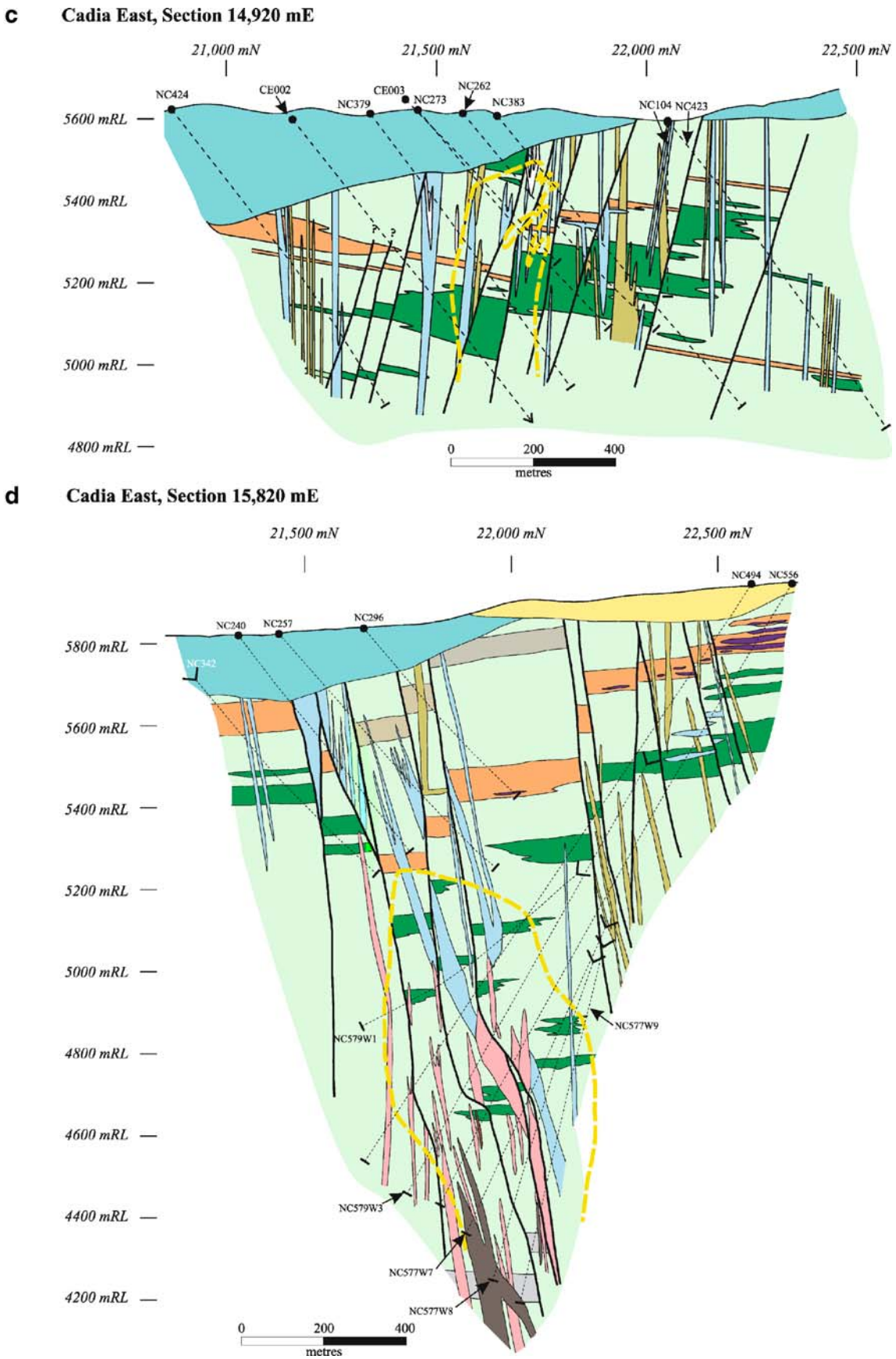

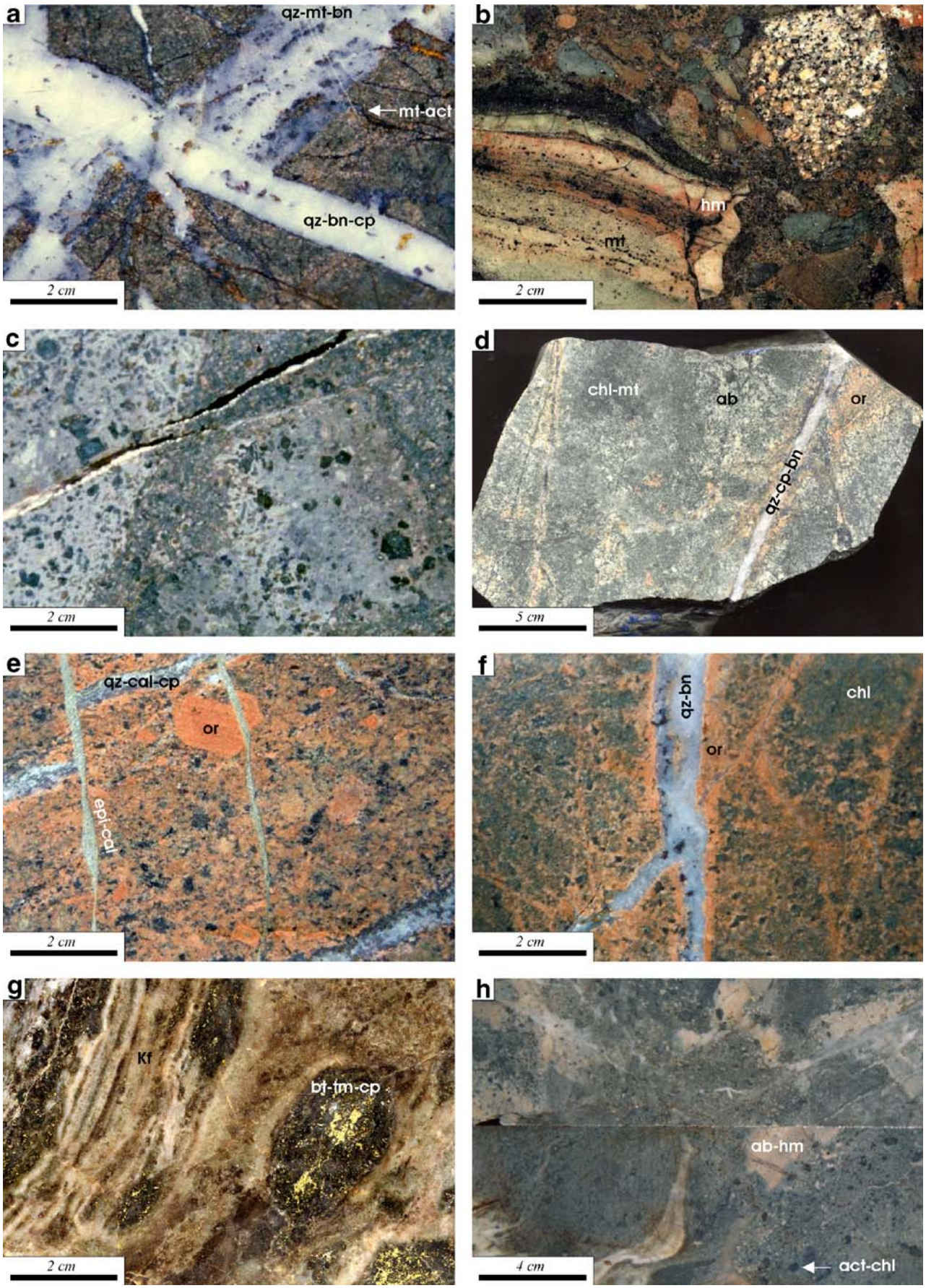
a
qz-mt-bn
mt-act
qz-bn-cp
2 cm
b
hm
mt
2 cm
c
2 cm
d
chl-mt
ab
or
qz-cp-bn
5 cm
e
qz-cal-cp
or
epi-cal
2 cm
f
qz-bn
or
chl
2 cm
g
Kf
bt-tm-cp
2 cm
h
ab-hm
act-chl
4 cm

◀ **Fig. 5** Porphyry-related alteration and mineralization of the Cadia district. **a** Pervasive calc–potassic- (actinolite–biotite–orthoclase) altered volcaniclastic sandstone with multiple generations of magnetite–actinolite and quartz–magnetite–bornite–chalcopyrite veins. Ridgeway, drill hole NC526W, 1,053.3 m. **b** Selectively pervasive inner propylitic (chlorite–albite–hematite–magnetite) alteration of clasts and matrix in a polymict volcanic conglomerate. Fine-grained hematite has dusted the feldspathic component of the rock, and ferromagnesian minerals have been altered to chlorite–epidote–magnetite. Ridgeway, drill hole NC498, 233.6 m. **c** Selectively pervasive outer propylitic (chlorite–albite–calcite) alteration of an andesite clast volcanic conglomerate. The feldspathic component of the clasts has been selectively altered to albite, whereas ferromagnesian phenocrysts are chlorite-altered. Ridgeway, drill hole NC523, 253.1 m. **d** Weakly plagioclase– and clinopyroxene–phyric basalt from the Forest Reefs Volcanics with pervasive propylitic (chlorite–magnetite) alteration and selective sodic (albite) and potassic (orthoclase; potassic II) alteration envelopes around magnetite–chlorite and quartz–chalcopyrite–bornite veins respectively. Cadia Hill open pit sample. **e** Reddened coarse grained orthoclase quartz monzonite porphyry. Quartz–calcite–chalcopyrite veins with orthoclase alteration envelopes (potassic II) have been cut by epidote veinlets with hematite alteration envelopes. Cadia Hill, drill hole NC076, 157.0 m. **f** Plagioclase–phyric basaltic andesite dyke that has been pervasively altered to fine-grained chlorite. Conspicuous quartz–bornite–chalcopyrite veins are associated with orthoclase alteration envelopes (potassic II). Cadia East, drill hole NC559W1, 1,226.5 m. **g** Fine-grained laminated siltstone with pervasive biotite–chalcopyrite–tourmaline alteration (potassic III) that has been partially overprinted by pervasive, late stage feldspar–quartz alteration. Cadia East, drill hole NC267, 302.5 m. **h** Clinopyroxene–phyric basalt that has been overprinted by irregular domains of inner propylitic alteration assemblage albite–hematite. Where recognizable, clinopyroxene phenocrysts have been altered to chlorite ± actinolite. Cadia East, drill hole NC494, 448.8 m. *ab* albite; *act* actinolite; *bn* bornite; *bt* biotite; *cal* calcite; *chl* chlorite; *cp* chalcopyrite; *epi* epidote; *hm* hematite; *Kf* K-feldspar; *mt* magnetite; *qz* quartz; *tm* tourmaline

using the paragenetic framework provided by Harper (2000), Wilson (2003), and Wilson et al. (2003, 2004). We use these data to assess (1) spatial variations in sulfide isotopic compositions, (2) the physicochemical conditions and mechanisms of sulfide deposition, and (3) the source(s) of sulfur in the ore forming fluids (e.g., Ohmoto and Rye 1979).

Previous work

There has been only one previous sulfur isotope study of sulfide minerals from the Cadia district. Green (1999) analyzed sulfide minerals from the Big Cadia skarn, and reported values of $\delta^{34}S_{pyrite}$ from −5.4 to +5.3‰ and $\delta^{34}S_{chalcopyrite}$ values between −5.1 and +2.9‰. No spatial zonation of $\delta^{34}S$ was identified. The range in $\delta^{34}S$ was interpreted to be due to isotopic exchange between an oxidized magmatic fluid and volcanic wallrocks that had a relatively heavy $\delta^{34}S$ composition. Carbon and oxygen isotopic data from Big Cadia hydrothermal calcite and unaltered limestone from the Forest Reefs Volcanics have $\delta^{13}C$ and $\delta^{18}O$ compositions consistent with mixing of hydrothermal fluids of magmatic origin with seawater at ~350°C Green (1999). Modeling of the calculated $\delta^{18}O_{fluid}$ values showed that the measured $\delta^{18}O_{magnetite}$ and $\delta^{18}O_{calcite}$ values could be produced from fluids circulating at temperatures of 250–450°C (Green 1999). Forster and Seccombe (2004) concluded that magmatic–hydrothermal fluids dominated skarn formation in the Cadia district, based on oxygen, deuterium, strontium, and carbon isotope analyses of gangue minerals. A minor seawater or meteoric contribution to the Little Cadia skarn was inferred based on the isotopic composition of secondary epidote (Forster and Seccombe 2004).

This study

One hundred and twelve sulfide samples were analyzed from different vein stages and alteration zones at Ridgeway (n=43), Cadia Hill (n=28), and Cadia East (n=41). Sulfate minerals (e.g., anhydrite and gypsum) are not present at Cadia and hence could not be analyzed. The relatively coarse grained nature of the sulfides enabled monomineralic powders to be hand-drilled. Sulfur isotopic analyses were completed at both the Central Science Laboratory at the University of Tasmania (Hobart, Australia) and at the United States Geological Survey (USGS) Isotope Laboratory in Denver (Colorado, USA). Ninety-three sulfide powders were analyzed at the University of Tasmania by conventional methods using the techniques of Robinson and Kusakabe (1975). An analytical uncertainty of ±0.1‰ was estimated from internal standards of homogenous galena from Broken Hill ($\delta^{34}S$=+3.40‰) and Rosebery ($\delta^{34}S$=+1.83‰) that were run with an SO_2 reference gas of $\delta^{34}S \approx$ Cañon Diablo Troilite (CDT). These internal standards were calibrated against international sphalerite standards IAEA NZ1 ($\delta^{34}S$=+1.83‰) and NBS 123 ($\delta^{34}S$=+4.34‰). Isotope measurements were performed on a VG Sira Series II mass spectrometer. Nineteen $\delta^{34}S$ analyses were performed at the USGS laboratory using an on-line method with an elemental analyzer coupled to a Micromass Optima mass spectrometer following the method of Giesemann et al. (1994).

Ridgeway

Results of forty-three analyses of sulfide minerals from Ridgeway are listed in Table 2 and illustrated in Fig. 6a. The $\delta^{34}S_{sulfide}$ values range between −5.7 and +9.2‰, with most between −4 and −1‰. The sulfur isotopic compositions of pyrite (n=24) range from −4.0 to +9.2‰, whereas chalcopyrite (n=17) and bornite (n=2) have more restricted ranges (−5.7 to −0.3‰ and −4.3 to −3.1‰, respectively; Fig. 6a).

There is a well-developed sulfur isotopic zonation pattern at Ridgeway (Fig. 7). The deposit core is characterized by isotopically light $\delta^{34}S_{bornite}$ and $\delta^{34}S_{chalcopyrite}$ values (average values of −3.7 and −2.9‰, respectively), which are preserved in sulfide minerals hosted by the quartz vein stockwork. Inner propylitic alteration assemblages that occur peripheral to this zone of quartz veining contain pyrite with relatively heavy $\delta^{34}S$ compositions (average −0.7‰). An anomalously high $\delta^{34}S_{pyrite}$ value

Table 2 Sulfur isotopic compositions, expressed as $\delta^{34}S$ values, for sulfide minerals from the Ridgeway porphyry Au–Cu deposit

Drill hole	Depth	Mineral	$\delta^{34}S$ (‰)	Alteration zone/vein stage
NC498	192.0	Pyrite-V/D	−2.4	Inner propylitic
NC498	352.8	Pyrite-D	−0.9	Inner propylitic
NC498	580.0	Chalcopyrite-V	−3.2	E-4
NC498	669.6	Chalcopyrite-D	−0.5	T-1
NC500	87.0	Pyrite-D	−1.2	Outer propylitic
NC500	131.0	Pyrite-D	−2.0	Inner propylitic
NC500	297.7	Pyrite-D	+0.8	Inner propylitic
NC500	315.0	Pyrite-D	+1.0	Inner propylitic
NC500	536.0	Chalcopyrite-D	−2.1	T-1
NC500	549.9	Chalcopyrite-V	−2.3	T-1
NC500	549.9	Pyrite-V/D	−0.6	T-1
NC500	613.0	Chalcopyrite-V	−0.3	T-1
NC500	679.3	Bornite-V	−3.1	E-4
NC500	679.3	Chalcopyrite-V	−2.6	E-4
NC500	788.1	Chalcopyrite-V	−3.1	T-1
NC500	905.0	Chalcopyrite-D	−2.4	T-1
NC500	1,191.5	Pyrite-D	−2.6	Calc-silicate
NC502	289.4	Pyrite-V	−1.6	Inner propylitic
NC502	352.8	Pyrite-V	−3.3	Py stringer
NC503	167.2	Pyrite-D	−0.7	Sodic
NC503	295.2	Pyrite-D	−1.9	Outer propylitic
NC503	672.0	Chalcopyrite-V	−4.0	T-1
NC503	867.0	Chalcopyrite-V	−5.7	T-1
NC510	192.0	Pyrite-D	+9.2	Sodic
NC510	376.1	Pyrite-D	−4.0	Outer propylitic
NC510	400.5	Pyrite-V	−0.8	Py vein
NC510	458.8	Pyrite-D	+1.1	Outer propylitic
NC510	539.9	Pyrite-V	+2.4	Qtz-py vein
NC510	840.8	Bornite-V	−4.3	E-4
NC553	83.5	Pyrite-D	−2.2	Inner propylitic
NC553	123.1	Pyrite-V/D	−1.7	Inner propylitic
NC553	159.2	Pyrite-D	−0.8	Inner propylitic
NC553	278.5	Pyrite-D	−2.1	Inner propylitic
NC553	328.1	Chalcopyrite-V	−3.4	Py-cp vein
NC553	328.1	Pyrite-D	−0.3	Py-cp vein
NC553	596.3	Chalcopyrite-V/D	−4.4	T-1
NC553	718.3	Chalcopyrite-V	−3.0	P-1 or T-1
NC553	721.0	Chalcopyrite-V	−3.1	T-1
NC553	721.0	Pyrite-V	−1.9	T-1
NC553	785.0	Chalcopyrite-V	−2.7	T-1
NC553	826.8	Chalcopyrite-V	−2.8	T-1
NC553	876.9	Pyrite-V	+0.6	L-1[a]
NC553	1,067.1	Chalcopyrite-V/D	−3.2	T-1

All samples analyzed at the University of Tasmania Central Science Laboratory, Hobart, Tasmania. Paragenetic stages from Wilson et al. (2003)

[a]This data point has not been plotted on Fig. 7, as it represents the late stage of the paragenetic sequence in the core of the Ridgeway deposit, whereas the other data are from the transitional and early stage veins

(+9.2‰) was obtained from pyrite within the sodic alteration zone peripheral to the upper parts of the Ridgeway system (Fig. 7).

Cadia Hill

The results of 28 $\delta^{34}S$ analyses from Cadia Hill are listed in Table 3 and illustrated in Fig. 6b. Cadia Hill has the largest range of sulfur isotopic compositions analyzed from the Cadia district, with the $\delta^{34}S_{sulfide}$ values ranging between −9.8

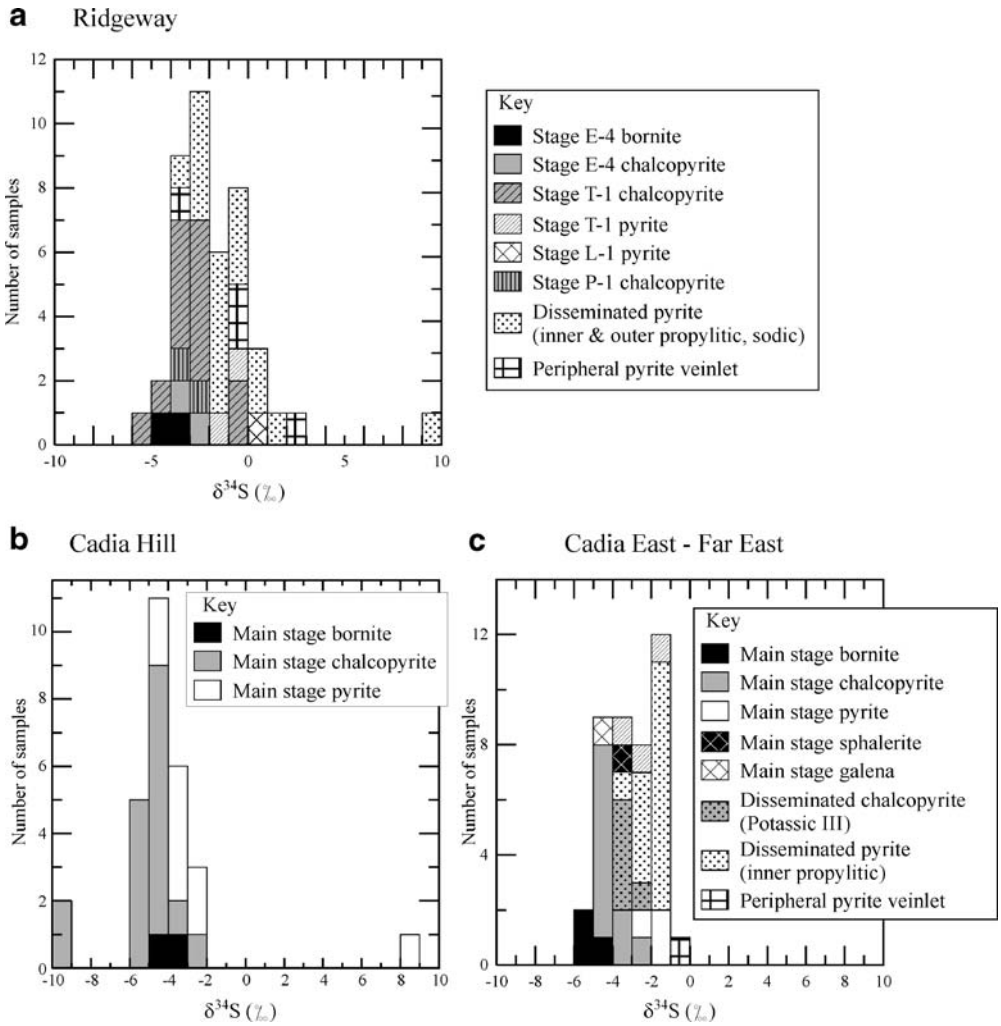

Fig. 6 Cumulative frequency plots of $\delta^{34}S$ values (per mil, relative to CDT standard) for sulfides from **a** Ridgeway, **b** Cadia Hill, and **c** Cadia East. Sulfides have been classified according to mineralogy and also by paragenetic stage/alteration assemblage. Ridgeway vein paragenesis from Wilson et al. (2003)

and +9.1‰. Pyrite compositions (n=10) cover the full range of data, whereas chalcopyrite compositions (n=16) are more restricted (−9.4 to −2.9‰; Fig. 6b). Bornite (n=2) has $\delta^{34}S$ values of −4.4 and −3.3‰ (Fig. 6b).

A systematic zonation of $\delta^{34}S_{sulfide}$ values is evident in the Cadia Hill deposit (Fig. 8). The central portion of the main stage vein envelope is dominated by isotopically light chalcopyrite (n=16, −9.4 to −2.9‰, with most below −4‰), and is surrounded by a zone of generally ^{34}S enriched pyrite (eight samples with $\delta^{34}S_{sulfide}$ values between −4.7 and −2.8‰). Bornite from the upper part of the main stage vein envelope is enriched in ^{34}S relative to chalcopyrite from the central portion of the envelope (Fig. 8). A single high $\delta^{34}S_{pyrite}$ value (+9.1‰) was obtained from pyrite from the propylitic-altered margin of Cadia Hill, approximately 150 m outside of the main stage vein envelope.

Cadia East

The results of 41 $\delta^{34}S$ analyses from Cadia East are listed in Table 4 and illustrated in Fig. 6c. The $\delta^{34}S_{sulfide}$ values range between −5.4 and −1.0‰. Bornite (n=3) has the lowest $\delta^{34}S$ values (−5.4 to −4.0). Pyrite compositions (n=21) range from −3.1 to −0.8‰, and chalcopyrite compositions (n=15) are between −4.9 and −2.6‰ (Fig. 6c). Coexisting grains of sphalerite ($\delta^{34}S$=−3.4‰) and galena ($\delta^{34}S$=−4.3‰) from a main stage quartz–calcite–sulfide vein have isotopic compositions similar to chalcopyrite.

The lowest $\delta^{34}S$ values at Cadia East occur in copper sulfides associated with all stages of potassic alteration (Table 4). Pyrite tends to be more enriched in ^{34}S than other Cadia East sulfide minerals, irrespective of the associated alteration assemblage. The $\delta^{34}S_{pyrite}$ compositions obtained from pyrite hosted within main stage veins (potassic II; Figs. 9 and 10) are similar to pyrite from the inner propylitic and late stage feldspar ± sodic alteration zones, and from quartz–pyrite veins on the deposit periphery (Table 4).

There is a well-developed zonation of $\delta^{34}S_{sulfide}$ values at Cadia East (Figs. 9 and 10). As at Ridgeway, the lowest $\delta^{34}S_{sulfide}$ values occur in the potassic-altered core of the deposit, and near-zero values occur in the peripheral propylitic alteration zones (Figs. 9 and 10). On section 14,920 mE, main stage quartz–calcite–sulfide veins from the deposit core have an average $\delta^{34}S_{chalcopyrite}$ value of −4.9‰. Disseminated chalcopyrite mineralization in the

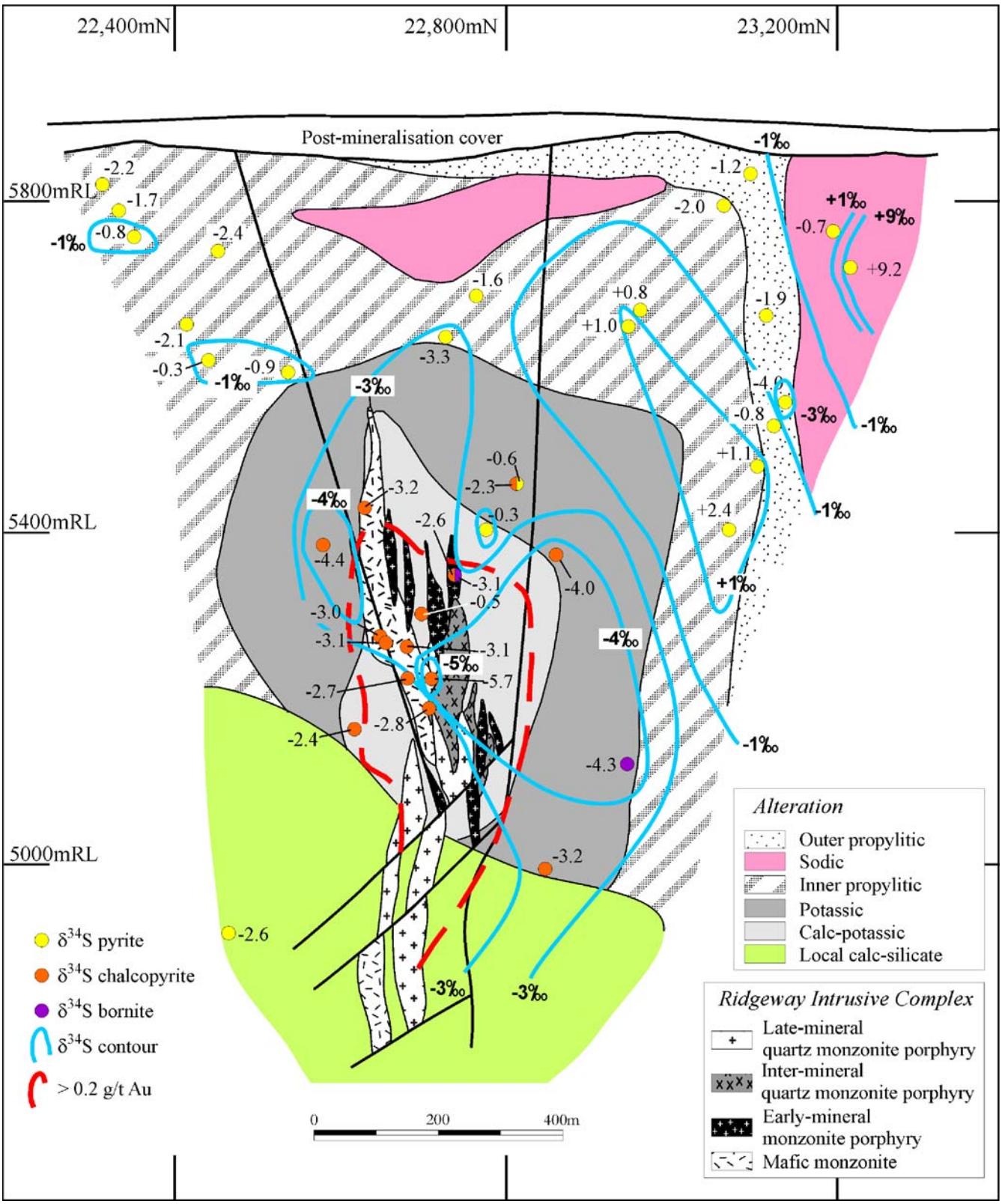

Fig. 7 Contoured values of $\delta^{34}S_{sulfide}$ values (per mil) from section 11,050 mE, Ridgeway. Also shown are the locations of the Ridgeway Intrusive Complex, the hydrothermal alteration zones that are developed around the intrusive complex, and the position of the 0.2 g/t gold grade contour

Table 3 Sulfur isotopic compositions, expressed as $\delta^{34}S$ values, for sulfide minerals from the Cadia Hill porphyry Au–Cu deposit

Drill hole	Depth	Mineral	$\delta^{34}S$ (‰)	Vein stage
NC075[b]	70.3	Chalcopyrite	−5.1	Main stage qtz–cal–sul vein
NC075[a]	139.4	Chalcopyrite	−4.5	Main stage qtz–cal–sul vein
NC075[b]	201.9	Pyrite	−4.6	Main stage qtz–cal–sul vein
NC075[b]	245.3	Pyrite	−3.7	Main stage qtz–cal–sul vein
NC076[b]	20.2	Chalcopyrite	−5.4	Main stage qtz–cal–sul vein
NC076[b]	99.8	Chalcopyrite	−5.2	Main stage qtz–cal–sul vein
NC076[b]	153.0	Chalcopyrite	−5.2	Main stage qtz–cal–sul vein
NC076[b]	181.1	Chalcopyrite	−4.9	Main stage qtz–cal–sul vein
NC076[a]	238.2	Pyrite	−4.0	Main stage qtz–cal–sul vein
NC099[b]	137.0	Pyrite	−3.6	Main stage qtz–cal–sul vein
NC099[b]	241.6	Chalcopyrite	−4.7	Main stage qtz–cal–sul vein
NC099[a]	293.6	Chalcopyrite	−4.8	Main stage qtz–cal–sul vein
NC099[a]	541.3	Pyrite	−2.8	Main stage qtz–cal–sul vein
NC099[b]	582.6	Chalcopyrite	−4.6	Main stage qtz–cal–sul vein
NC142[b]	103.1	Pyrite (trace only)	+9.1	Main stage qtz–cal–sul vein
NC142[b]	276.3	Pyrite	−2.9	Main stage qtz–cal–sul vein
NC142[b]	345.6	Chalcopyrite	−4.3	Main stage qtz–cal–sul vein
NC142[a]	676.9	Pyrite	−3.2	Main stage qtz–cal–sul vein
NC152[a]	35.2	Bornite	−3.3	Main stage qtz–cal–sul vein
NC152[a]	125.8	Bornite	−4.4	Main stage qtz–cal–sul vein
NC185[b]	162.3	Chalcopyrite	−3.4	Main stage qtz–cal–sul vein
NC203[b]	74.3	Chalcopyrite	−4.8	Main stage qtz–cal–sul vein
NC203[a]	182.0	Chalcopyrite	−4.5	Main stage qtz–cal–sul vein
NC203[b]	240.9	Chalcopyrite	−9.4	Main stage qtz–cal–sul vein
NC203[b]	282.3	Chalcopyrite	−5.4	Main stage qtz–cal–sul vein
NC203[b]	369.6	Pyrite	−9.8	Main stage qtz–cal–sul vein
NC203[b]	446.2	Pyrite	−4.7	Main stage qtz–cal–sul vein
NC205[a]	124.4	Chalcopyrite	−2.9	Main stage qtz–cal–sul vein

cal Calcite, *qtz* quartz, *sul* sulfide
[a]Analyzed at the University of Tasmania Central Science Laboratory, Hobart, Tasmania
[b]Analyzed at the United States Geological Survey Isotope Laboratory, Denver, Colorado

upper, biotite-altered portion of the deposit has a slightly heavier isotopic composition ($\delta^{34}S_{chalcopyrite}$=−4.0 to −3.0‰, average −3.7‰). Pyrite from the peripheral, inner propylitic alteration zone has higher $\delta^{34}S$ values (−2.8 to −1.1‰, average −1.6‰) and similar $\delta^{34}S_{pyrite}$ values (−3.1 to −0.8‰, average −2.0‰) were obtained from the late stage, near surface feldspar alteration zone.

On section 15,820 mE, isotopically light bornite ($\delta^{34}S$= −5.4 to −4.0‰, average −4.9‰) and chalcopyrite ($\delta^{34}S$= −4.5 to −2.6‰, average −3.8‰) in main stage veins are surrounded by inner propylitic and skarn alteration assemblages that contain isotopically heavier pyrite ($\delta^{34}S$=−2.1 to −1.0‰, average −1.6‰). Main stage quartz–calcite–sulfide veins that occur on the margins of the 0.2 g/t Au grade boundary have heavier $\delta^{34}S$ compositions ($\delta^{34}S_{chalcopyrite}$=−2.6‰, $\delta^{34}S_{pyrite}$=−2.8‰) than sulfides from similar veins in the central and deeper portions of the deposit.

Discussion

This study has shown that systematic sulfur isotopic zonation patterns characterize Ridgeway, Cadia Hill, and Cadia East, and that these patterns coincide broadly with the previously documented sulfide and alteration zonation (Figs. 7, 8, 9 and 10). The high-grade mineralized cores of the deposits are characterized by the lowest $\delta^{34}S_{sulfide}$ values, with a return to near-zero values on the deposit peripheries. Similar results have been obtained from alkalic porphyry deposits at Mt Polley (Deyell 2005) and Afton (Deyell and Tosdal 2005) in British Columbia, and at Goonumbla in NSW (Heithersay and Walshe 1995; Radclyffe 1995; Lickfold 2002). The following discussion explains the origin of these isotopic zonation patterns, infers the likely source(s) of sulfur, and speculates on fluid compositions and processes of ore formation.

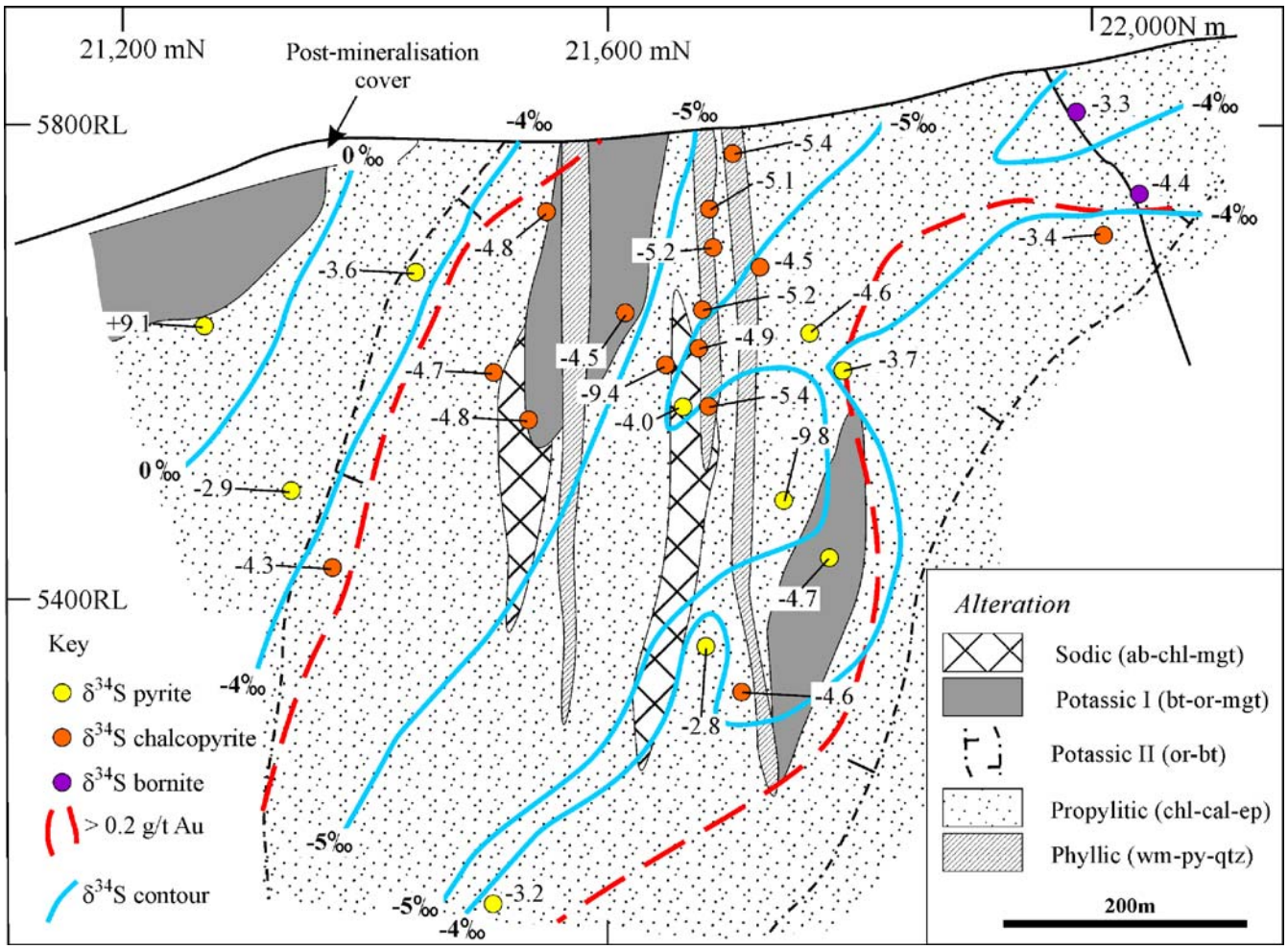

Fig. 8 Contoured values of $\delta^{34}S_{sulfide}$ values (per mil) from section 14,020 mE, Cadia Hill. All samples are from quartz–calcite–sulfide veins with orthoclase (potassic II) alteration halos. Also shown is the 0.2 g/t gold grade contour. *ab* albite; *bt* biotite; *cal* calcite; *chl* chlorite; *ep* epidote; *mgt* agnetite; *or* orthoclase; *py* pyrite; *qtz* quartz; *wm* white mica

Sulfur source and fluid compositions

Typical ranges of $\delta^{34}S_{sulfide}$ and $\delta^{34}S_{sulfate}$ values from porphyry deposits are −3 to +1‰ and +8 to +15‰, respectively (Fig. 11). Most of the $\delta^{34}S_{sulfide}$ data obtained from the Cadia porphyry deposits are between −9.8 and +2.4‰ (Tables 2, 3 and 4). Although the data from Cadia extends well below the normal range, it is comparable to other porphyry deposits of alkalic character (e.g., E26N, Galore Creek, Red Chris, and Dinkidi; Fig. 11).

The excursions to anomalously low $\delta^{34}S_{sulfide}$ values in the core of each of the Cadia deposits can either be explained by magmatic–hydrothermal processes, or by incorporation of an external, isotopically light, sulfur source such as biogenic sulfide, which is characteristically depleted in ^{34}S (Ohmoto and Rye 1979). Shannon et al. (1983) proposed that interaction of a magmatic–hydrothermal fluid with a biogenic sulfur source resulted in the low $\delta^{34}S_{sulfide}$ compositions at Galore Creek in British Columbia. At Cadia, there is no local biogenic sulfur source—the volcano-sedimentary wallrocks to the Cadia deposits are devoid of sedimentary sulfides (Fig. 3). It is therefore concluded that sulfur at Cadia is primarily of magmatic derivation. This is consistent with the magmatic source of sulfur inferred for the nearby E26N deposit at Goonumbla (Fig. 2; Heithersay and Walshe 1995), where $\delta^{34}S_{sulfide}$ values as low as −19‰ have been detected (Lickfold 2002).

H_2S and SO_2 are the predominant sulfur species that occur in high temperature (>400°C) magmatic fluids typical of porphyry copper deposits (Rye 1993). At temperatures below 400–350°C, aqueous sulfate can be generated according to the following hydrolysis reaction (Holland 1965; Rye et al. 1992):

$$4\,H_2O + 4\,SO_2 \Rightarrow H_2S + 3\,H^+ + 3\,HSO_4^- \quad (1)$$

Under equilibrium conditions, the ^{34}S isotope will preferentially fractionate into the oxidized sulfur species (Ohmoto and Rye 1979) such that sulfides deposited from oxidized magmatic fluids will be preferentially depleted in ^{34}S, and will have low $\delta^{34}S$ values (Rye 1993). Under highly oxidizing conditions (e.g., H_2S/SO_4=0.2, Fig. 12a),

Table 4 Sulfur isotopic compositions, expressed as $\delta^{34}S$ values, for sulfide minerals from the Cadia East porphyry Au–Cu deposit

Drill hole	Depth	Mineral	$\delta^{34}S$ (‰)	Alteration zone/vein stage
CE002	487.0	Pyrite	−1.5	Inner propylitic
CE002	712.1	Chalcopyrite	−4.9	Main stage qtz–cal–sul
CE002	830.6	Chalcopyrite	−4.9	Main stage qtz–cal–sul
CE003	132.3	Pyrite	−2.3	Late stage feldspar
CE003	279.0	Chalcopyrite	−3.9	Potassic III
CE003	546.4	Chalcopyrite	−4.4	Main stage qtz–cal–sul
NC240	385.2	Pyrite	−1.9	Potassic III
NC240	593.3	Chalcopyrite	−4.2	Main stage qtz–cal–sul
NC267	283.0	Chalcopyrite	−3.8	Main stage qtz–cal–sul
NC267	449.0	Chalcopyrite	−4.5	Main stage qtz–cal–sul
NC267	612.9	Chalcopyrite	−3.8	Potassic I
NC296	191.3	Pyrite	−1.1	Late stage feldspar
NC296	254.8	Pyrite	−1.2	Late stage feldspar
NC296	519.0	Pyrite	−2.1	Skarn
NC342	539.4	Pyrite	−1.1	Main stage qtz–cal–sul
NC342	744.6	Pyrite	−2.8	Main stage qtz–cal–sul
NC379	226.9	Pyrite	−0.8	Py–chl vein
NC379	338.9	Pyrite	−2.2	Potassic III
NC379	473.2	Chalcopyrite	−4.3	Main stage qtz–cal–sul
NC379	571.4	Sphalerite	−3.4	Main stage qtz–cal–sul
NC379	571.4	Galena	−4.3	Main stage qtz–cal–sul
NC383	192.1	Chalcopyrite	−3.0	Potassic III
NC383	521.2	Chalcopyrite	−4.0	Potassic I
NC423	16.8	Pyrite	−3.1	Late stage feldspar
NC423	165.9	Pyrite	−2.8	Inner propylitic
NC424	356.3	Pyrite	−3.0	Skarn
NC424	551.7	Pyrite	−1.0	Main stage qtz–cal–sul
NC424	779.9	Pyrite	−1.1	Inner propylitic
NC494	214.0	Pyrite	−1.3	Skarn
NC494	390.3	Pyrite	−1.3	Inner propylitic
NC494	595.3	Pyrite	−1.9	Inner propylitic
NC494	696.5	Pyrite	−1.0	Inner propylitic
NC494	1,506.0	Pyrite	−1.5	Inner propylitic
NC556	899.0	Pyrite	−2.1	Inner propylitic
NC556	1,108.0	Chalcopyrite	−2.6	Main stage qtz–cal–sul
NC556	1,312.8	Chalcopyrite	−3.8	Main stage qtz–cal–sul
NC556	1,452.0	Bornite	−4.0	Main stage qtz–cal–sul
NC577W8	1,403.5	Chalcopyrite	−4.1	Main stage qtz–cal–sul
NC577W8	1,546.2	Bornite	−5.4	Main stage qtz–cal–sul
NC579W1	1,087.3	Bornite	−5.4	Main stage qtz–cal–sul
NC579W1	1,133.4	Chalcopyrite	−3.4	Main stage qtz–cal–sul

All samples analyzed at the University of Tasmania Central Science Laboratory, Hobart, Tasmania
cal Calcite, *qtz* quartz, *sul* sulfide

cooling of a magmatic fluid will result in a wide range of $\delta^{34}S_{sulfide}$ values that become increasingly depleted in heavy sulfur with cooling. A narrow range of $\delta^{34}S_{sulfate}$ values will be produced under oxidizing conditions. In contrast, the range of $\delta^{34}S_{sulfide}$ values produced under reducing conditions (e.g., H_2S/SO_4=5, Fig. 12b) will be small, and the range of $\delta^{34}S_{sulfate}$ values will be large (Rye 1993). Temporal and/or spatial variations of the sulfur isotopic compositions of minerals in magmatic–hydrothermal systems are therefore thought to reflect changes in temperature and/or oxidation state (H_2S/SO_4) of fluids after magmatic exsolution, assuming a constant composition of bulk sulfur ($\delta^{34}S_{\Sigma S}$) in the system (Ohmoto and Rye 1979; Rye 1993). Over the temperature range typical of porphyry copper deposits (600 to 300°C), sulfur isotopic fractionation between the sulfide mineral pairs observed at Cadia (pyrite-chalcopyrite and chalcopyrite-bornite) is predicted to account for isotopic shifts of only 0.3 to 1.4‰ (Fig. 12). By itself, cooling of the magmatic–hydrothermal fluids,

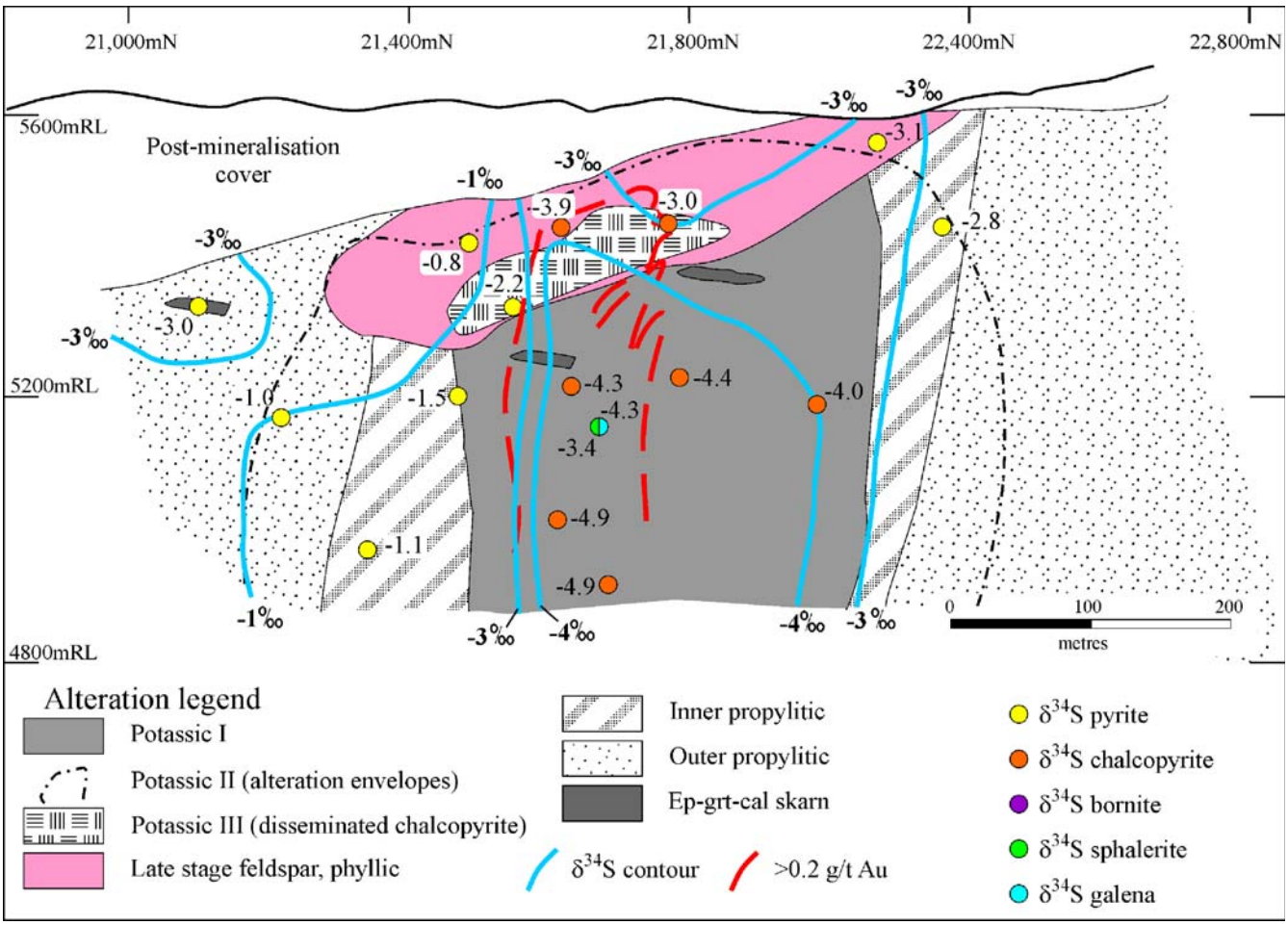

Fig. 9 Contoured values of $\delta^{34}S_{sulfide}$ values (per mil) from section 14,920 mE, Cadia East. Also shown is the distribution of hydrothermal alteration on this section, in addition to the main 0.2 g/t gold grade contour. *cal* calcite; *ep* epidote; *gt* garnet

therefore, cannot explain the excursion to distinctly negative $\delta^{34}S_{sulfide}$ values in the core of the Cadia deposits, and another explanation is required.

By integrating the results of sulfur isotope analyses with estimated temperatures of precipitation of sulfur-bearing minerals, information may be gained about the H_2S/SO_4 value and the bulk $\delta^{34}S$ composition of the ore fluid (Ohmoto and Rye 1979; Rye 1993). Previous fluid inclusion studies have shown that early-stage magmatic–hydrothermal fluids in the Cadia porphyry systems had temperatures from 400°C to more than 600°C and salinities from 49 to 62 eq. wt‰ NaCl (Wilson 2003; Wilson et al. 2003). These physicochemical conditions are typical of porphyry systems worldwide. Oxidizing fluid conditions are consistent with the widespread development of ferric iron-bearing minerals (e.g., hematite, magnetite, and epidote) within the alteration halos at Cadia (e.g., Fig. 5). Consequently, the low $\delta^{34}S_{bornite}$ and $\delta^{34}S_{chalcopyrite}$ values that characterize the mineralized quartz veins in the core of the Cadia porphyry deposits (Figs. 7, 8, 9 and 10), are interpreted to be a product of sulfide deposition from oxidized (sulfate-predominant), high temperature magmatic–hydrothermal fluids (e.g., Fig. 12a).

Two anomalously high values of $\delta^{34}S_{pyrite}$ have been detected on the fringes of Ridgeway and Cadia Hill (+9.2 and +9.1‰, respectively). These pyrites could not have been precipitated from the oxidized magmatic–hydrothermal fluids that produced the main sulfide assemblages at Cadia (e.g., Fig. 12a). Instead, another fluid may have been involved in sulfide precipitation. The subwave base depositional environment for the Weemalla Formation and the Forest Reefs Volcanics is consistent with a submarine volcanic setting. Green (1999) argued that the carbon–oxygen isotope systematics of the Big Cadia skarn were consistent with mixing of magmatic–hydrothermal fluids with seawater. The anomalously high sulfur isotopic compositions of pyrite from Ridgeway and Big Cadia are therefore interpreted to be the product of minor sulfide deposition from a seawater-derived fluid ($\delta^{34}S_{Ordovician\ seawater} \approx +25‰$; Ohmoto and Rye 1979). Marine sulfate either resided as connate porewater within

Fig. 10 Contoured values of $\delta^{34}S_{sulfide}$ values (per mil) from section 15,820 mE, Cadia East. Also shown is the distribution of hydrothermal alteration on this section and the location of the Cadia East intrusive complex, in addition to the main 0.2 g/t gold grade contour. *ab* albite; *bt* biotite; *cal* calcite; *ccp* chalcopyrite; *ep* epidote; *gt* garnet, *mgt* magnetite; *or* orthoclase; *py* pyrite

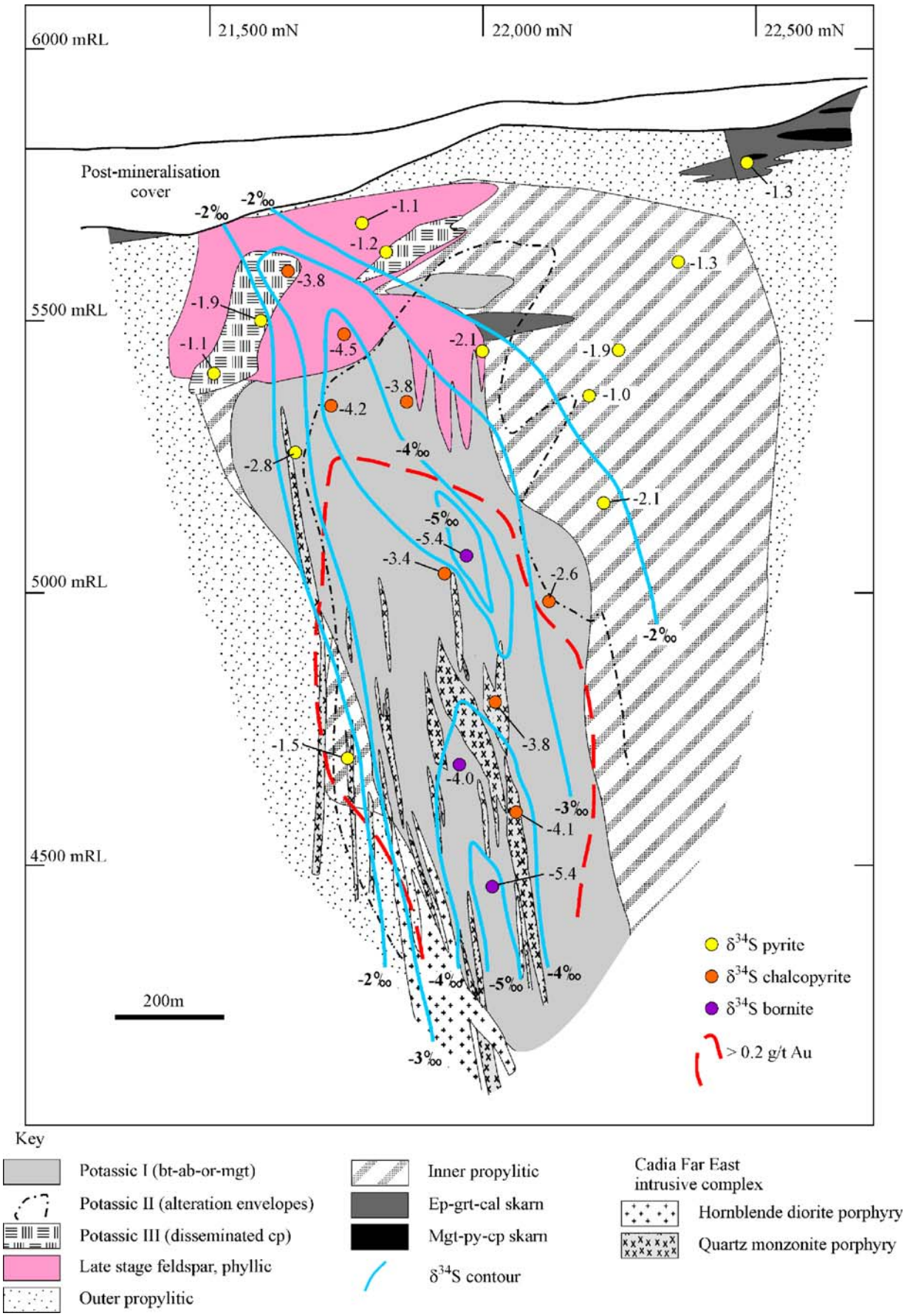
6000 mRL
21,500 mN
22,000 mN
22,500 mN
Post-mineralisation cover
5500 mRL
5000 mRL
4500 mRL
-2‰
-4‰
-5‰
-3‰
200m
δ34S pyrite
δ34S chalcopyrite
δ34S bornite
> 0.2 g/t Au
Key
Potassic I (bt-ab-or-mgt)
Potassic II (alteration envelopes)
Potassic III (disseminated cp)
Late stage feldspar, phyllic
Outer propylitic
Inner propylitic
Ep-grt-cal skarn
Mgt-py-cp skarn
δ34S contour
Cadia Far East intrusive complex
Hornblende diorite porphyry
Quartz monzonite porphyry

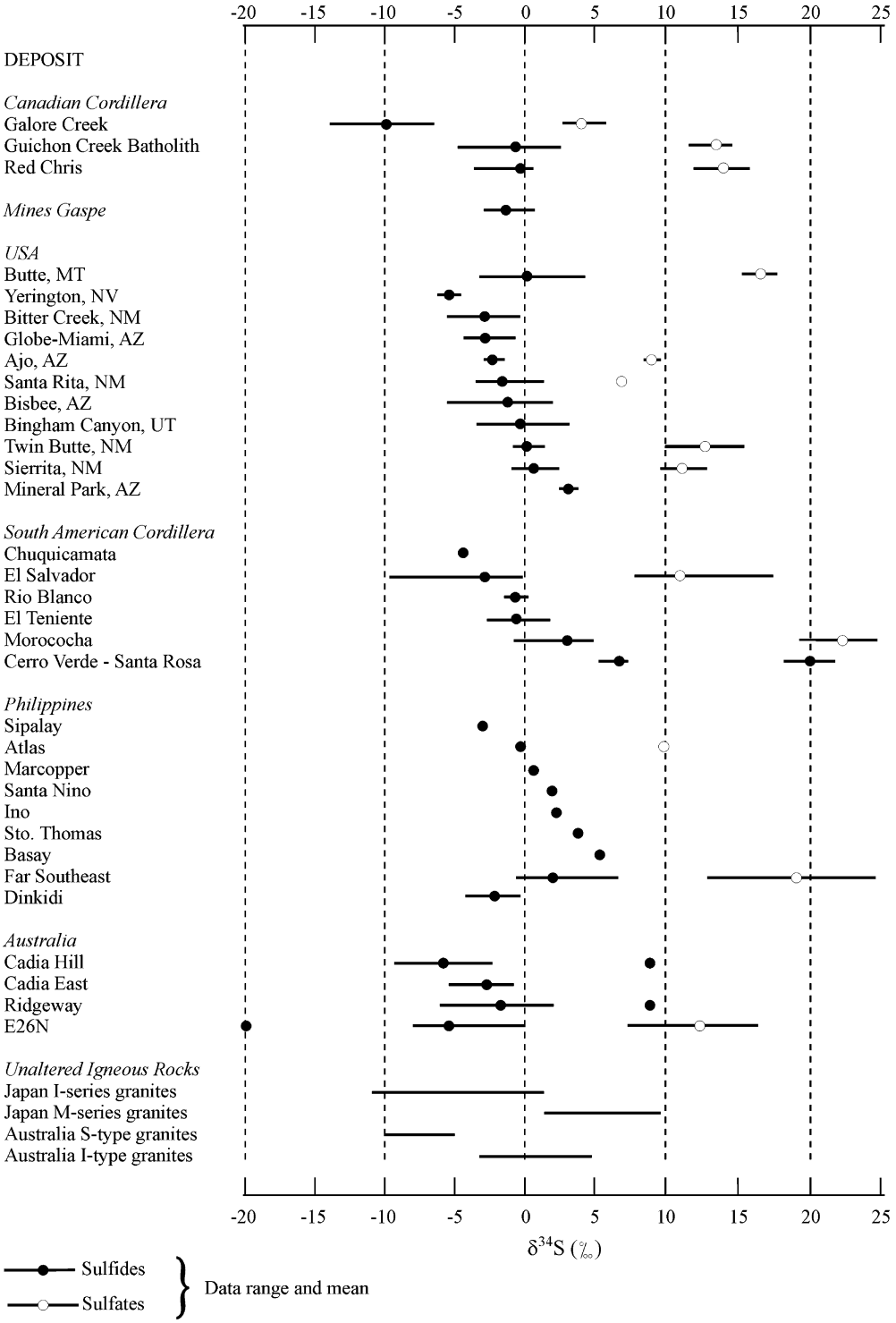

Fig. 11 Ranges of $\delta^{34}S_{sulfide}$ values (per mil) determined for sulfide and sulfate minerals associated with porphyry copper (–gold) deposits, and with granitic rocks. Data for the Cadia deposits are from this study. Other data sources are Ohmoto and Rye (1979), Taylor (1987), Heithersay and Walshe (1995), Baker and Thompson (1998), Akira (2000), Wolfe (2001), and Lickfold (2002). The two anomalously high pyrite $\delta^{34}S_{sulfide}$ values from Ridgeway and Cadia Hill and an anomalously low value from E26N are plotted as single points, to emphasize how they are distinct from the main data range

the Forest Reefs Volcanics, or could have been circulating convectively on the periphery of the Cadia systems. The isotopic evidence for seawater involvement in the Cadia systems is extremely limited (e.g., Cooke et al. 2007), and so this process is not considered to have been important for ore formation.

Water-rock interaction and sulfate reduction

The zonation of $\delta^{34}S_{sulfide}$ values at Cadia, from the lowest values in the core of the deposits to higher values on the periphery (Figs. 7, 8, 9 and 10) cannot be explained simply by sulfide deposition from a cooling, oxidized magmatic hydrothermal fluid (e.g., Fig. 12a). This zonation pattern requires that the oxidation state and/or the bulk sulfur

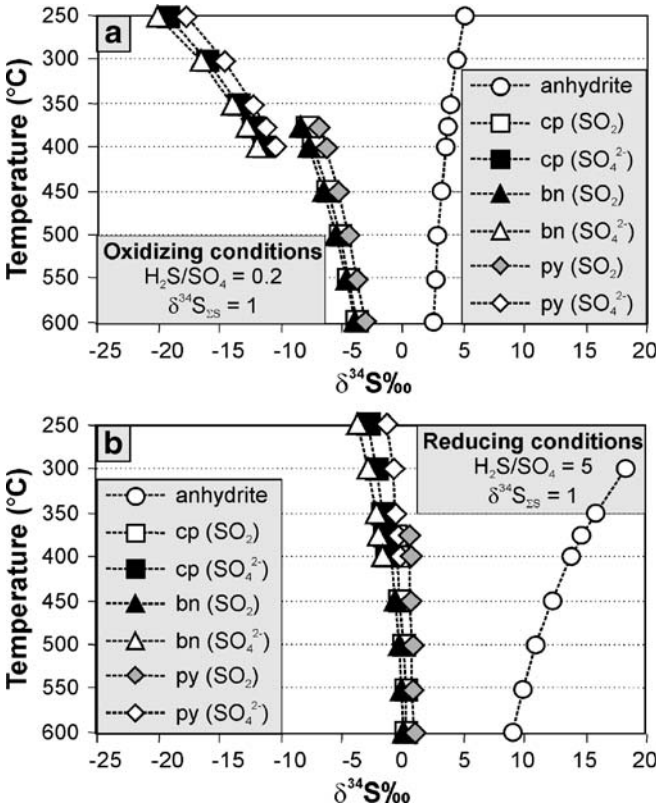

Fig. 12 Idealized $\delta^{34}S$ behavior of coexisting sulfide and sulfate minerals precipitated from a cooling hydrothermal fluid of magmatic origin with an initial bulk sulfur composition ($\delta^{34}S_{\Sigma S}$) of 1, under **a** oxidizing conditions and **b** reducing conditions. Calculations based on the work of Rye (1993) and use average $\delta^{34}S_{sulfide}$ data from this study. Anhydrite compositions are calculated values assuming a closed isotopic system and an infinite sulfur reservoir. At temperatures of <400–350°C, SO_4^{2-} becomes the most important oxidized sulfur species in the aqueous fluid

isotopic composition of the mineralizing fluid changed during sulfide deposition at Cadia.

In an attempt to explain the possible causes behind the observed $\delta^{34}S_{sulfide}$ zonation patterns at Cadia, the effects that changing H_2S/SO_4 and $\delta^{34}S_{\Sigma S}$ compositions can have on $\delta^{34}S_{sulfide}$ compositions during cooling have been modeled using the sulfide–sulfate fractionation equation of Ohmoto and Lasaga (1982). This modeling requires estimates for the temperatures of sulfide deposition. Fluid inclusion analyses have determined that the principal stages of quartz veining at Cadia East, Cadia Hill, and Ridgeway were deposited at minimum temperatures of 400–450°C (Wilson 2003; Wilson et al. 2003). The temperature of formation of disseminated pyrite in the inner and outer propylitic alteration zones has not been established. However, propylitic (albite–chlorite–epidote) alteration assemblages have been interpreted to form at 250–350°C by Reed (1997), with the presence of hematite and epidote indicating formation at the high end of this temperature range (Beane and Titley 1981). Consequently, disseminated pyrite in the inner and outer propylitic alteration zones is considered to have been deposited at ~300°C. This is consistent with the findings of Green (1999), who reported a formation temperature of ~350°C for pyrite associated with epidote–calcite alteration at Big Cadia.

The average $\delta^{34}S$ values for sulfides in the deposit core at Ridgeway are −3.7‰ (bornite), −2.8‰ (chalcopyrite), and −1.3‰ (pyrite; Fig. 13a). Based on the fluid inclusion study of coexisting quartz grains by Wilson et al. (2003), their average depositional temperature was approximately 450°C. At Cadia Hill and Cadia East (Fig. 13b,c), the average $\delta^{34}S_{sulfide}$ compositions in the core of the systems are −3.9 and −4.9‰ (bornite), −5.2 and −4.1‰ (chalcopyrite), and −2.3 and −1.6‰ (pyrite), respectively. A depositional temperature of approximately 400°C is assumed for these two systems based on the fluid inclusion results of Wilson (2003). By using the above temperature constraints, and assuming conditions of isotopic equilibrium, these $\delta^{34}S$ compositions could be produced at 400–450°C by a cooling magmatic fluid with a $\delta^{34}S_{\Sigma S}$ of 2‰ and an H_2S/SO_4 of 1 (Model 1, Fig. 13d). At 300°C, disseminated pyrite at Ridgeway and Cadia East has an average $\delta^{34}S$ composition of −0.7 and −1.8‰, respectively. Simple cooling of the above-mentioned magmatic fluid, however, would produce pyrite at 300°C with a $\delta^{34}S$ composition of −6.9‰ (Fig. 13d), indicating that cooling alone cannot produce the observed isotopic zonation patterns.

It is possible to produce the measured $\delta^{34}S_{pyrite}$ compositions at Cadia under changing redox conditions during cooling. For the conditions shown in Fig. 13e, an increase in the H_2S/SO_4 value from 1 to 4 during cooling from 450 to 300°C is required. One mechanism to increase this ratio is via the inorganic reduction of sulfate by reaction with ferrous iron in the wallrock to produce sulfide. Ohmoto and Lasaga (1982) studied the kinetics of aqueous sulfates and sulfides in hydrothermal systems and concluded that the rate of inorganic sulfate reduction, although dependant on temperature, pH, and total sulfate concentration, appears to be fast enough to become geologically important at temperatures above 200°C.

Aqueous sulfate that has been produced by SO_2 disproportionation (reaction 1) can potentially undergo reduction due to reaction of the sulfate-bearing water with primary ferrous iron-bearing minerals that are common throughout the Forrest Reefs Volcanics, such as clinopyroxene or magnetite (which contains both ferrous and ferric iron) or FeO from volcanic glass. Huston et al. (2001) proposed such a process to account for the high $\delta^{34}S$ values of pyrite in a zone of leached volcanic rocks in the Panorama volcanic-hosted massive sulfide district of Western Australia. At Cadia Hill, Cadia East, and Ridge-

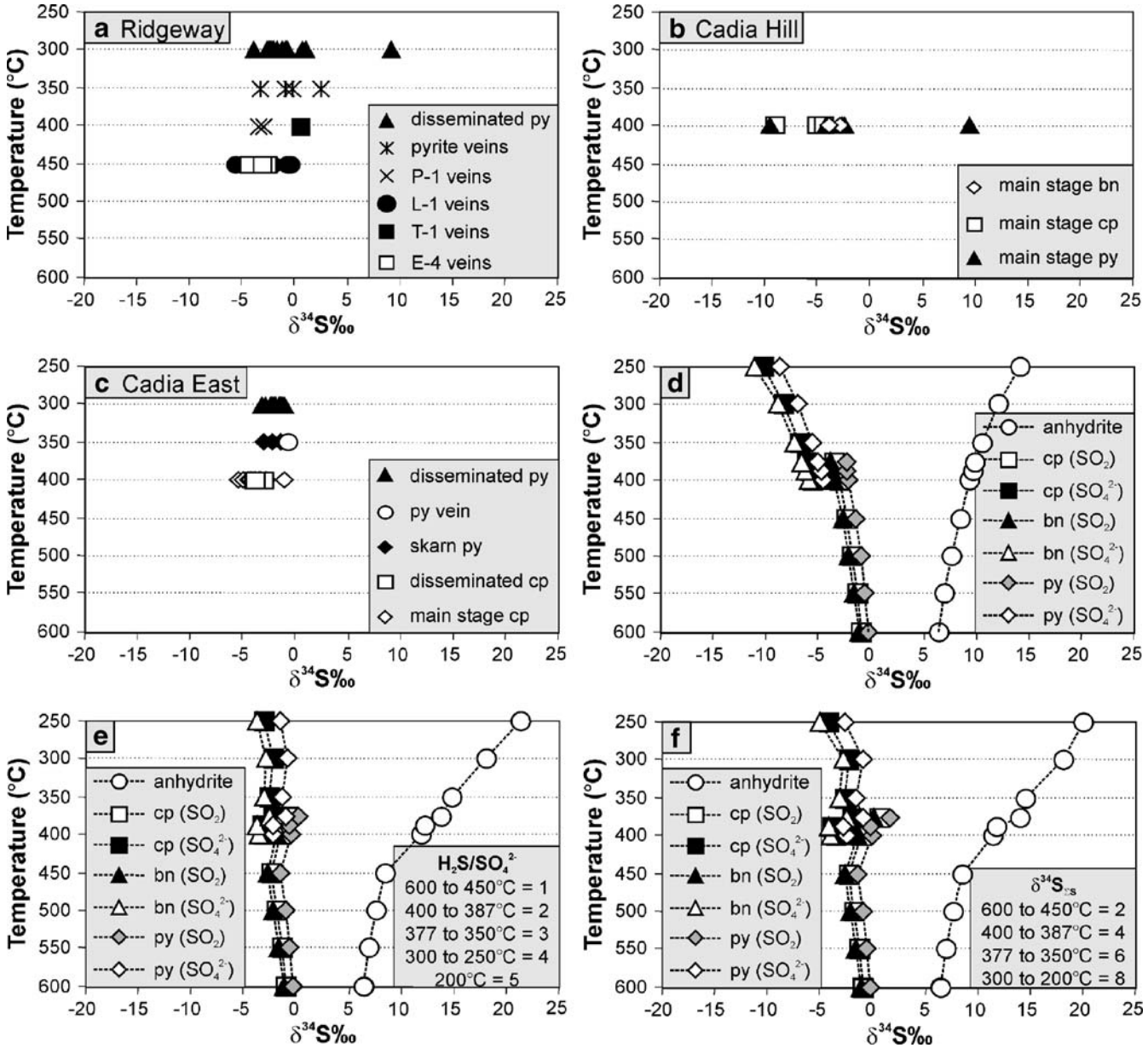

Fig. 13 Measured (**a**, **b** and **c**) and modeled (**d**, **e** and **f**) $\delta^{34}S_{sulfide}$ compositions of the Ridgeway, Cadia Hill, and Cadia East porphyry deposits. Temperature estimates used in **a**, **b** and **c** based on the fluid inclusion study of Wilson (2003) and from mineralogical constraints. **a** Sulfur isotopic compositions of sulfide minerals at Ridgeway. **b** Sulfur isotopic compositions of sulfide minerals at Cadia Hill. **c** Sulfur isotopic compositions of sulfide minerals at Cadia East. **d** Theoretical sulfide and sulfate $\delta^{34}S$ values calculated for minerals precipitated from a fluid that contains equal proportions of oxidized and reduced sulfur (H_2S/SO_4=1) with a bulk $\delta^{34}S$ value of 2‰, plotted as a function of temperature. The bulk $\delta^{34}S$ value was selected arbitrarily to best fit the measured sulfide compositions and fluid inclusion temperatures. **e** Theoretical sulfide and sulfate $\delta^{34}S$ values calculated for minerals precipitated from a fluid that evolves to more reducing conditions during cooling (H_2S/SO_4 evolves from one to five) with a bulk $\delta^{34}S$ value of 2‰, plotted as a function of temperature. **f** Theoretical sulfide and sulfate $\delta^{34}S$ values calculated for minerals precipitated from a fluid that has a constant aqueous sulfate/sulfide ratio (1), but a bulk $\delta^{34}S$ composition that increased from two to eight with decreasing temperature. All theoretical sulfide compositions are calculated using sulfide-SO_2 fractionation equations above 350°C, and sulfide-SO_4^{2-} fractionation equations below 400°C, to allow for the effects of disproportionation of $SO_{2(g)}$ to $SO_4^{2-}(aq)$ (Rye 1993)

way, the presence of ferric iron-bearing minerals (e.g., hematite, magnetite, and epidote; Fig. 5) in the zone of ^{34}S-enriched pyrite provide mineralogical support for the occurrence of inorganic sulfate reduction. For example, hematite may be produced in the following fashion:

$$8\,FeO_{(rock)} + SO_4^{2-}(aq) + 2\,H^+_{(aq)} \Leftrightarrow 4\,Fe_2O_{3(s)} + H_2S_{(aq)} \quad (2)$$

and magnetite may form by a similar reaction:

$$12\,FeO_{(rock)} + SO_4^{2-}(aq) + 2\,H^+_{(aq)} \Leftrightarrow 4\,Fe_3O_{4(s)} + H_2S_{(aq)} \quad (3)$$

whereas epidote can form by the replacement of clinopyroxene as follows:

$$\begin{aligned} CaFe^{2+}Si_2O_{6(s)} + SO_4^{2-}(aq) + 2A1(OH)_{3(aq)} \\ +H_4SiO_{4(aq)} + 2H^+_{(aq)} \\ \Leftrightarrow CaFe^{3+}A1_2Si_3O_{12}(OH)_{(s)} + H_2S_{(aq)} \\ +4.5\,H_2O_{(1)} + 1.25O_{2(aq)} \end{aligned} \quad (4)$$

In reactions 2, 3, and 4, aqueous sulfate is reduced to sulfide at the same time that ferrous iron is oxidized to ferric iron. These reactions, which appear to typify the propylitic alteration zones at Cadia, can provide H_2S that is enriched in ^{34}S relative to the oxidized mineralizing fluids, and can explain the reversal of $\delta^{34}S_{sulfide}$ compositions.

Interaction with an external sulfur reservoir

An alternative method for producing the zonation patterns of $\delta^{34}S$ at Cadia involves the interaction of the mineralizing fluids with an external reservoir enriched in ^{34}S. Such a process would cause the bulk $\delta^{34}S_{\Sigma S}$ value of the mineralizing fluids to change, potentially resulting in a reversal of the trend towards lower $\delta^{34}S_{sulfide}$ values predicted for simple cooling of an oxidized fluid (Fig. 12a).

We have attempted to simulate the effects of changing the bulk sulfur isotopic composition of the mineralizing fluid by arbitrarily increasing the $\delta^{34}S_{\Sigma S}$ value for the mineralizing fluid incrementally from 2 to 8‰ during cooling from 600 to 200°C (Model 3, Fig. 13f). Our calculations show that changing the bulk sulfur isotopic composition of the fluid during cooling could produce the isotopic zonation patterns observed at Cadia.

The mafic to intermediate volcanic wallrocks that host the Cadia deposits are a possible external source of sulfur. We suspect that these rocks probably have a bulk $\delta^{34}S$ value of around +4‰, based on $\delta^{34}S$ data from Tertiary island arc volcanic rocks of the western Pacific (Ueda and Sakai 1984). However, the mafic to intermediate Forest Reefs Volcanics are not sulfidic away from the mineralized centers at Cadia. They are not sulfate-bearing and so they are unlikely to have been a major sulfur reservoir at the time of mineralization. Furthermore, the estimated $\delta^{34}S$ composition of the volcanic wallrocks is lower than the $\delta^{34}S_{\Sigma S}$ of the fluid required to produce the range of $\delta^{34}S_{sulfide}$ compositions observed in the deposits. It therefore seems unlikely that incorporation of sulfur from the Forest Reefs Volcanics could explain the isotopic zonation patterns at Cadia.

Mixing with Ordovician seawater ($\delta^{34}S \approx +25$‰; Ohmoto and Rye 1979) could have changed the bulk sulfur isotopic composition of the mineralizing fluid, as shown in Fig. 13f. However, the stable and radiogenic isotopic evidence for seawater involvement at Cadia is limited (i.e., $\delta^{34}S_{pyrite}$ values of +9.2 and +9.1‰ obtained from the upper margins of the Ridgeway and Cadia Hill deposits—Figs. 7 and 8; carbon–oxygen data from Big Cadia skarn—Green 1999). Furthermore, the strontium isotopic compositions of epidote from Big Cadia and Cadia Hill are primitive, ruling out the presence of a large component of seawater-derived strontium (Cooke et al. 2007). Oxygen–deuterium analyses of muscovite from late-stage fault zones indicate a predominance of magmatic–hydrothermal fluids, and provide no evidence for seawater involvement (Wilson 2003). It is therefore concluded that fluid mixing with seawater is unlikely to have been important for generating the sulfur isotopic zonation patterns at Cadia, but may explain the two anomalously high $\delta^{34}S_{pyrite}$ values on the periphery of Ridgeway and Cadia East.

Conclusions and exploration implications

The high-grade ore zones in the Cadia porphyry deposits are characterized by ^{34}S-depleted sulfides that were deposited from oxidized (sulfate-predominant) magmatic–hydrothermal fluids. Progressive enrichment in $^{34}S_{sulfide}$ compositions with distance upwards and outwards from the mineralized centers (Figs. 7, 8, 9 and 10) was most likely caused by sulfate reduction during the processes of water–rock interaction. This also resulted in the reddened, hematite-, and epidote-rich propylitic alteration halos to the Cadia ore deposits. A minor contribution of seawater sulfate in the peripheral alteration zones at Ridgeway and Cadia Hill may have occurred; although detailed oxygen-deuterium isotopic analyses of propylitic alteration minerals are required to further evaluate this hypothesis.

Recognition of distinctive isotopic zonation patterns in the Cadia porphyry deposits has significant implications for the exploration of alkalic porphyry systems. Porphyry mineralization is associated with magmatically derived sulfur, which typically has near-zero $\delta^{34}S$ values (Ohmoto 1986; Taylor 1987; Fig. 12). However, when the mineralizing fluids contain abundant sulfate, sulfide deposition can result in isotopic fractionation towards progressively lower $\delta^{34}S_{sulfide}$ values (Fig. 12a). At Cadia, this resulted in $\delta^{34}S_{sulfide}$ values of −4 to −10‰ within the high-grade mineralized cores of the deposits. More extreme fractionation appears to have occurred at the nearby E26 alkalic porphyry (Goonumbla; Fig. 2), where $\delta^{34}S_{sulfide}$ values as low as −19‰ have been detected (Lickfold 2002; Fig. 11). It is also possible that similar processes resulted in the strongly depleted $\delta^{34}S_{sulfide}$ values detected at Galore Creek in British Columbia (Shannon et al. 1983; Fig. 11).

We propose that sulfur isotopic analyses of pyrite should be considered as a potential tool to assist future drilling programs in alkalic porphyry provinces. This technique has the potential to allow explorers in propylitically altered rocks to identify when they are proximal to areas affected by oxidizing magmatic–hydrothermal fluids (i.e. the

mineralized core of the ore system). At Ridgeway, Cadia Hill, and Cadia East, this type of mineralizing fluid produced excursions to more negative pyrite sulfur isotopic compositions in the propylitic halo outside of the potassically altered and copper-mineralized ore zones, and we predict that similar behavior is likely in other alkalic porphyry systems.

Acknowledgements Our work at Cadia has benefited immensely from the input of Newcrest's exploration and mine geologists, and we particularly want to thank John Holliday, Ian Tedder, Paul Dunham, and Tully Richards for their on-going support and advice. This work was carried out as part of a Ph.D. study by AJW and an honors project by BH at the Centre for Ore Deposit Research (CODES), and we gratefully acknowledge the Director of CODES, Professor Ross Large, for his on-going support and financial assistance. We also thank Garry Davidson for assistance with the isotopic modeling and Simon Stephens for thin section preparation. Bob Rye (USGS) and Keith Harris and Christine Cook (U. Tasmania) are thanked for undertaking sulfur isotopic analyses. The reviews of Thomas Ulrich and John Walshe helped to improve this document considerably. We thank Newcrest Mining Limited for the permission to publish these results. CODES is the Australian Research Council's Centre of Excellence in Ore Deposits.

References

Akira I (2000) Mineral paragenesis, fluid inclusions and sulfur isotope systematics of the Lepanto Far South East porphyry Cu–Au deposit, Mankayan, Philippines. Resour Geol 50:151–168

Baker T, Thompson JFH (1998) Fluid evolution at the Red Chris porphyry Cu–Au deposit, Northwest British Columbia. Geol Soc Am, Abstracts with Programs 30:367

Beane RE, Titley SR (1981) Porphyry copper deposits, Part II. Hydrothermal alteration and mineralization. In: Skinner BJ (ed) Economic Geology 75th Anniversary Volume. Economic Geology Publishing Company, El Paso, pp 235–269

Cooke DR, Wilson AJ, House MJ, Wolfe RC, Walshe JL, Lickfold V, Crawford AJ (2007) Alkalic porphyry Au–Cu and associated mineral deposits of the Ordovician to Early Silurian Macquarie Arc, NSW. Aust J Earth Sci (in press)

Cooper RA (1999) The Ordovician timescale—calibration of graptolite and conodont zones. Acta Univ Carol Geol 43:1–4

Deyell CL (2005) Sulfur isotope zonation at the Mt Polley alkalic porphyry Cu–Au deposit, British Columbia, Canada. In: Mao J, Bierlein FP (eds). Mineral deposit research: meeting the global challenge (8th Biennial SGA meeting), pp 373–376

Deyell CL, Tosdal R (2005) Sulfur isotopic zonation in alkalic porphyry Cu–Au systems II: applications to mineral exploration in British Columbia. geological fieldwork: a summary of field activities and current research, 2005–1, pp 191–208

Drummond AD, Godwin CI (1976) Hypogene mineralization: an empirical evaluation of alteration zoning. Canadian Institute of Mining and Metallurgy, Special vol 15, pp 52–63

Forster DB, Seccombe PK (2004) Oxygen, hydrogen, carbon and strontium isotope characteristics of the Cadia porphyry–skarn deposits, New South Wales, Australia. In: McPhie J, McGoldrick P (eds) Dynamic Earth: past, present and future. Geol Soc Austr, Abstracts 73:77–78

Giesemann A, Jager HJ, Norman AL, Krouse HR, Brand WA (1994) On-line sulfur–isotope determination using an elemental analyzer coupled to a mass spectrometer. Anal Chem 65:2816–2819

Glen RA, Walshe JL (1999) Cross-structures in the Lachlan Orogen: the Lachlan Transverse Zone example. Aust J Earth Sci 46:641–658

Green D (1999) Geology, geochemistry and genesis of the Big Cadia deposit, NSW. B.Sc. Honors thesis, University of Tasmania, Hobart, p 154

Harper BL (2000) Hydrothermal alteration at the Ridgeway porphyry gold–copper deposit, NSW. B.Sc. Honors thesis, University of Tasmania, Hobart, p 130

Heithersay PS, Walshe JL (1995) Endeavour 26 North: a porphyry copper–gold deposit in the Late Ordovician, shoshonitic Goonumbla volcanic complex, New South Wales, Australia. Econ Geol 90:1506–1532

Holland HD (1965) Some applications of thermochemical data to problems of ore deposits. II. Mineral assemblages and the composition of ore-forming fluids. Econ Geol 60:1101–1166

Holliday J, McMillan C, Tedder I (1999) Discovery of the Cadia Ridgeway gold–copper deposit: new generation gold mines—case histories of discovery. Australian Mineral Foundation, Perth, pp 101–107

Holliday JR, Wilson AJ, Blevin PL, Tedder IJ, Dunham PD, Pfitzner M (2002) Porphyry gold–copper mineralization in the Cadia district, eastern Lachlan Fold Belt, New South Wales, and its relationship to shoshonitic magmatism. Miner Depos 37:100–116

Huston DL, Brauhart CW, Drieberg SL, Davidson GJ, Groves DI (2001) Metal leaching and inorganic sulfate reduction in volcanic-hosted massive sulfide mineral systems: evidence from the paleo-Archean Panorama district, Western Australia. Geology 29:687–690

Lang JR, Stanley CR, Thompson JFH, Dunne KPE (1995) Na–K–Ca magmatic–hydrothermal alteration in alkalic porphyry Cu–Au deposits, British Columbia. In: Thompson JFH (ed) Magmas, fluids and ore deposits. Mineralogical Association of Canada Short Course, vol 23. Mineralogical Association of Canada, Victoria, pp 339–366

Lickfold V (2002) Intrusive history and volatile evolution of the Endeavour porphyry Cu–Au deposits, Goonumbla district, NSW, Australia. Ph.D. thesis, University of Tasmania, Hobart, p 243

Lickfold V, Cooke DR, Smith SG, Ullrich TD (2003) Endeavour Cu–Au porphyry deposits, Northparkes, NSW: intrusive history and fluid evolution. Econ Geol 98:1607–1636

Lowell JD, Guilbert JM (1970) Lateral and vertical alteration–mineralization zoning in porphyry ore deposits. Econ Geol 65:373–408

Newcrest Mining Limited (2004) Concise Annual Report, p 72

Newcrest Mining Staff (1996) The Cadia "wallrock–porphyry"-style gold–copper deposit, NSW. In: Porphyry-related copper and gold deposits of the Asia-Pacific region. Australian Mineral Foundation, Cairns, pp 16.1–16.10

Ohmoto H (1986) Stable isotope geochemistry of ore deposits. In: Valley JW, Taylor HP, O'Neil JR (eds) Stable isotopes in high temperature geological environments. Rev Miner 16:491–559

Ohmoto H, Lasaga AC (1982) Kinetics of reactions between aqueous sulfates and sulfides in hydrothermal systems. Geochim Cosmochim Acta 46:1727–1745

Ohmoto H, Rye RO (1979) Isotopes of sulfur and carbon. In: Barnes HL (ed) Geochemistry of hydrothermal ore deposits, 2nd edn. Wiley, New York, pp 509–567

Packham G, Percival I, Bischoff G (1999) Age constraints on strata enclosing the Cadia and Junction Reefs ore deposits of central New South Wales, and tectonic implications. Geol Surv N S W 110:1–12 Quarterly Notes

Radclyffe D (1995) Regional scale propylitic alteration in the North Parkes mineral field. B.Sc. honors thesis, University of Tasmania, Hobart, p118

Reed MH (1997) Hydrothermal alteration and its relationship to ore fluid composition. In: Barnes HL (ed) Geochemistry of hydrothermal ore deposits, 2nd edn. Wiley, New York, pp 303–365

Rickards RB, Percival IG, Simpson AJ, Wright AJ (2001) Silurian biostratigraphy of the Cadia area, south of Orange, New South Wales. Proc Linnean Soc N S W 123:173–191

Robinson BW, Kusakabe M (1975) Quantitative preparation of sulfur dioxide, for $^{34}S/^{32}S$ analyses, from sulfides by combustion with cuprous oxide. Anal Chem 47:1179–1181

Rye RO (1993) The evolution of magmatic fluids in the epithermal environment: the stable isotope perspective. Econ Geol 88: 733–752

Rye RO, Bethke PM, Wasserman WD (1992) The stable isotope geochemistry of acid sulfate alteration. Econ Geol 87:225–262

Shannon SSJ, Finch RJ, Ikramuddin M, Mutschler FE (1983) Possible sedimentary sources of sulfur and copper in alkaline-suite porphyry–copper systems. Geol Soc Am, Abstract with Programs 15:684

Taylor BE (1987) Stable isotope geochemistry of ore-forming fluids. In: Kyser TK (ed) Stable isotope geochemistry of low temperature processes. Mineralogical Association of Canada Short Course Handbook 13, Toronto, pp 337–445

Tedder IJ, Holliday J, Hayward S (2001) Discovery and evaluation drilling of the Cadia Far East gold–copper deposit. New generation gold deposits 2001 conference proceedings. Australian Mineral Foundation, Perth, pp 171–184

Titley SR (1982) The style and progress of mineralization and alteration in porphyry copper systems. In: Titley SR (ed) Advances in geology of the porphyry copper deposits, southwestern North America. The University of Arizona Press, Tucson, pp 93–116

Ueda A, Sakai H (1984) Sulfur isotope study of Quaternary volcanic rocks from the Japanese islands arc. Geochim Cosmochim Acta 48:1837–1848

Wilson AJ (2003) The geology, genesis and exploration context of the Cadia gold–copper porphyry deposits, New South Wales, Australia. Ph.D. thesis, University of Tasmania, Hobart, p 335

Wilson AJ, Cooke DR, Harper BL (2003) The Ridgeway gold–copper deposit: a high-grade alkalic porphyry deposit in the Lachlan Fold Belt, NSW, Australia. Econ Geol 98:1637–1656

Wilson AJ, Cooke DR, Richards T (2004) Veins, pegmatites and breccias: examples from the alkalic Cadia Quarry Au–Cu porphyry deposit, NSW, Australia. In: Cooke DR, Deyell C, Pongratz J (eds) 24 carat gold workshop: CODES special publication no. 5. University of Tasmania, Hobart, pp 45–56

Wolfe RC (2001) Geology of the Didipio region and paragenesis of the Dinkidi Cu–Au porphyry deposit. Ph.D. thesis, University of Tasmania, Hobart, p 200